CHAPTER 6

Basins associated with strike–slip deformation

On that day his feet will stand on the Mount of Olives, east of Jerusalem, and the Mount of Olives will be split in two from east to west, forming a great valley, with half of the mountain moving north and half moving south.

(ZECHARIAH 14:4, NEW INTERNATIONAL VERSION)

SUMMARY

Sedimentary basins generally form by localized extension along a strike–slip fault system which itself may be related to either divergent, convergent, or oblique relative plate motion. Less commonly, loading resulting from local crustal thickening may cause flexural subsidence. Although strike–slip basins form in a wide variety of geodynamical settings such as oceanic and continental transforms and arc and suture collisional boundaries, they are best known from intracontinental and continental margin environments.

In simple systems, the orientation of the strike–slip fault in relation to the plate slip vector is important in determining whether divergent (transtensile) or convergent (transpressive) strike–slip takes place. This guide breaks down, however, in complex regions of continental convergence such as Turkey.

Zones of strike–slip tectonics are characterized by active seismicity on strike–parallel and strongly oblique faults, with zones of infrequent, large earthquakes along locked segments, and frequent small earthquakes along unlocked segments. Some of the world's best known and most hazardous faults are strike–slip. Heat flows are generally low, suggesting that major strike–slip faults are weak and therefore generate little frictional heat. Geodetic surveys and paleomagnetic results show that small and large crustal blocks commonly rotate about a subvertical axis during strike–slip deformation. Characteristic geomorphic features result from the lateral displacement of adjacent terranes.

Sedimentary basins in zones of strike–slip deformation are diverse and complex. Some are clearly thin-skinned and related to extensional or contractional detachments in the weak lower crust. A number of different types of basin can be discriminated on the basis of kinematic setting, chief of which are fault bend basins, overstep basins, transrotational and transpressional basins.

The bulk of the shear strain is accommodated in a central *principal displacement zone* (PDZ) which may be linear to curvilinear in plan view and steeply inclined in section. The PDZ commonly branches upwards into a splaying system of faults producing a *flower structure*. Some fault zones, such as the Garlock Fault in California, penetrate to great depths, terminating in the middle crust, whereas others link at depth with relatively shallow low-angle detachments belonging to orogenic wedges. Strike–slip zones are characterized by *en echelon* arrangements of faults and folds that are orientated in a consistent pattern with respect to the strain ellipse. The most important fractures are termed *Riedel Shears*, but extension fractures are also formed. *En echelon* folds may form, with axes roughly at right angles to the extension fractures. The exact pattern of faults and folds produced in any particular fault zone depends on the local geological fabric and the youth or maturity of the fault system.

The precise structural pattern is controlled by a number of factors including: (i) the kinematics (convergent, divergent, parallel) of the fault system, (ii) the magnitude of the displacement, (iii) the material properties of the rocks and sedimentary infills in the deforming zone, and (iv) the configuration of pre-existing structures.

The PDZ is characteristically segmented. The individual segments may be linked, both in plan view and cross-sectional view, by *oversteps*. If the sense of an along-strike overstep is the same as the sense of fault slip, a *pull-apart basin* is formed: if the sense of the overstep is opposite to that of fault slip, a *push-up range* is formed. Pull-apart basins appear to develop in a continuous

evolutionary sequence at releasing bends with increasing offset, from narrow "spindle-shaped" basins to "lazy S" and "lazy Z" basins to "rhomboidal" basins and eventually into ocean-floored basins. However, the weakness of major strike–slip zones may cause transform-normal extension, producing markedly asymmetrical strike–slip basins. Numerical modeling of basins at stepovers using a basal forcing are successful at generating the broad features of pull-apart basins, such as the Dead Sea Basin.

Thermal and subsidence modeling is poorly developed in strike–slip basins, largely on account of their complex structural history. In basins involving lithospheric thinning, the uniform extension model has been applied with modifications for the lateral loss of heat through the basin walls during the extension. Other basins appear to form over zones of thin-skinned extension, with no mantle involvement. These basins, such as the Vienna Basin in the compressive Alpine–Carpathian system, are cool and lack a well-developed postextension thermal subsidence.

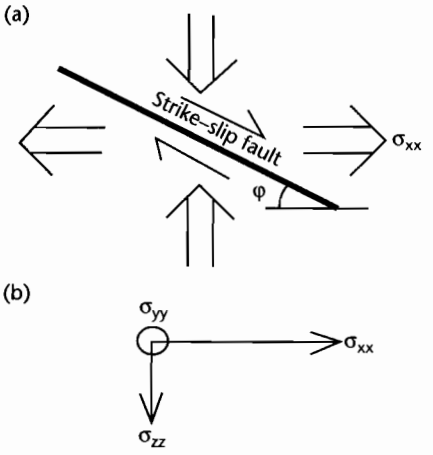

Fig. 6.1 Plane strain approximation for strike–slip faults. (a) Conjugate strike–slip faults at an angle φ to the principal stress σ_{xx}; (b) Principal stresses are related by $\sigma_{zz} > \sigma_{yy} > \sigma_{xx}$.

6.1 OVERVIEW

6.1.1 Geological and geophysical observations

Basins associated with strike–slip deformation are generally small and complex compared to cratonic sags, passive margins, and foreland basins. They are intimately linked to the detailed structural evolution of an area and mechanical models have been relatively slow to appear because of the extreme complexity of this history of deformation. Nevertheless, numerical 3-D models are available for basin development in particular structural settings within a zone of strike–slip deformation.

Strike–slip deformation occurs where principally lateral movement takes place between adjacent crustal or lithospheric blocks. In pure strike–slip, the displacement is purely horizontal, so there is no strain in the vertical dimension y. This is the situation of *plane strain*. The vertical stress in strike–slip faulting is the vertical lithostatic stress $\sigma_{yy} = \rho gh$. The horizontal stresses are the deviatoric stresses, one compressional, and the other extensional. The vertical stress is always the intermediate stress. Two conjugate strike–slip faults are anticipated from this state of stress, one right-lateral and the other left-lateral, inclined at an angle φ to the principal stress σ_{xx} (Fig. 6.1).

In reality, movement in strike–slip zones is rarely purely lateral, and displacements are commonly *oblique*, that is, involving a certain amount of normal or reverse dip–slip movement. Oblique slip may therefore characterize any strike–slip zone, but particular zones may experience a net contraction while others may suffer net extension. The stress regimes responsible for these two variants on pure strike–slip deformation are known as *transpressive* and *transtensile*.

Major strike–slip deformation and associated basin formation takes place in a wide range of geodynamic situations. Strike–slip zones may be associated with entire plate boundaries such as the San Andreas Fault system of California and the Alpine Fault system of New Zealand, microplate boundaries, intraplate deformations, or small fractures of limited displacement. Sylvester (1988), drawing considerably on Woodcock's (1986) genetic scheme (Fig. 6.2), proposed a classification of strike–slip faults into *interplate* and *intraplate* varieties (Table 6.1). He recommends use of the term "transform" fault for deep-seated interplate types and "transcurrent" fault for intraplate strike–slip faults confined to the crust. Of greatest importance to students of basin analysis are the strike–slip faults cutting continental lithosphere where uplifting and eroding source areas for sediment are available.

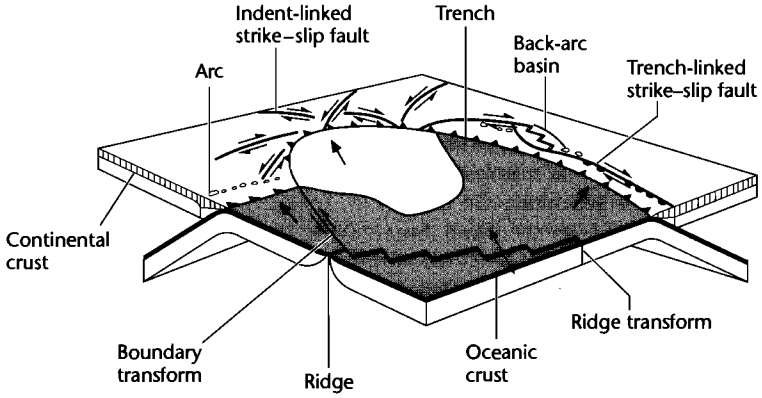

Fig. 6.2 Genetic classification of major classes of strike–slip fault according to plate tectonic setting (after Woodcock 1986). See also Table 6.1.

Table 6.1 Sylvester's (1988) classification of strike–slip faults.

1 **Interplate "transforms"** (deep-seated, delimiting plate)	2 **Intraplate "transcurrent" faults** (confined to crust)
1.1 *Ridge transform faults* Displace segments of oceanic crust with similar spreading vectors e.g., Romanche fracture zone (Atlantic Ocean)	2.1 *Indent-linked strike–slip faults* Bound continental blocks in collision zones e.g., North Anatolian (Turkey), Altyn Tagh, and Kunlun (Tibet)
1.2 *Boundary transform faults* Separate different plates parallel to the plate boundary e.g., San Andreas (California), Alpine Fault (New Zealand)	2.2 *Intracontinental strike–slip faults* Separate allochthons of different tectonic styles e.g., Garlock Fault (California)
1.3 *Trench-linked strike–slip faults* Accommodate horizontal component of oblique subduction e.g., Atacama Fault (Chile), Median Tectonic Line (Japan)	2.3 *Tear faults* Accommodate different displacement within a given allochthon or between the allochthon and adjacent structural units e.g., Asiak fold thrust belt (Canada)
	2.4 *Transfer faults* Linking overstepping or *en echelon* strike–slip faults e.g., Southern and Northern Diagonal Faults (eastern Sinai, Israel)

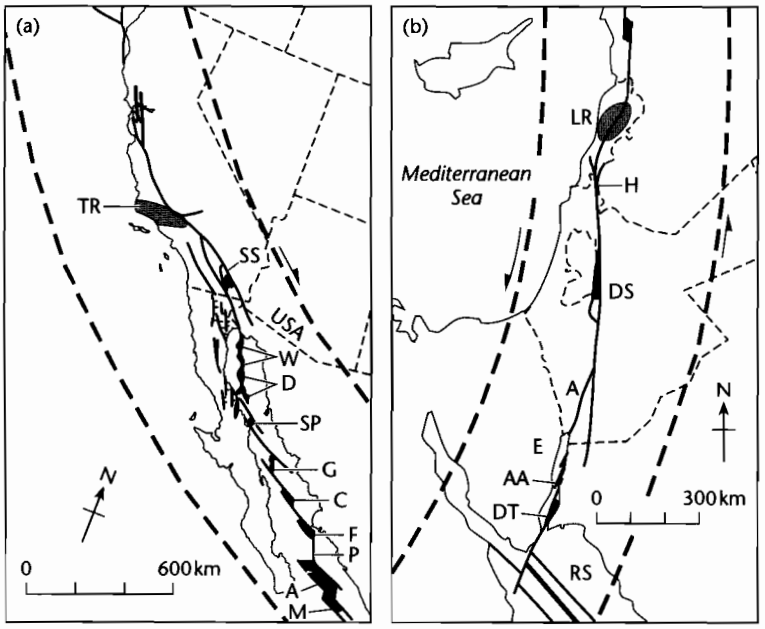

Fig. 6.3 Regions of compression and extension along strike–slip boundaries between rigid continental plates related to the orientation of the fault zone with respect to the plate slip vector (after Mann et al. 1983). (a) Pacific–North American Plate boundary. The dashed lines are theoretical interplate slip lines from Minster et al. (1974). The major zone of compression is the push-up block of the Transverse Ranges where the dextral San Andreas Fault Zone has a "convergent" orientation with respect to the interplate slip line. The prominent pull-apart basins, however, are situated relatively to the south where the fault zone has a "divergent" orientation with respect to the interplate slip line. TR, Transverse Ranges; SS, Salton Sea pull-apart as a right step between the San Andreas and Imperial Faults. Pull-aparts in the Gulf of California include: W, Wagner Basin; D, Delfin Basin; SP, San Pedro Martir Basin; G, Guaymas Basin; C, Carmen Basin; F, Farallon Basin; P, Pescadero Basin Complex; A, Alarcon Basin; M, Mazatlan Basin; (b) Arabia–Sinai (Levant) Plate boundary zone (Garfunkel 1981; Ben-Avraham et al. 1979). Theoretical interplate slip lines are from Le Pichon and Francheteau (1978). The prominent area of compression is the Lebanon Ranges push-up block where the sinistral Dead Sea Fault Zone is "convergent" with respect to the interplate slip lines. Most of the pull-apart basins are in the Dead Sea and Gulf of Aqaba regions where the fault zone is locally "divergent" with respect to the interplate slip lines. Pull-aparts include: H, Hula Basin; DS, Dead Sea Basin; A, Arava Fault Trough; E, Elat Basin in the northern Gulf of Aqaba; AA, Arnona–Aragonese Basin; DT, Dakar–Tiran Basin.

The development of regions of extension and shortening along strike–slip systems has been related to the relative orientation of the plate slip vectors and the major faults (Mann et al. 1983). In the case of the San Andreas and Dead Sea strike–slip systems, basins develop where the principal displacement zone is divergent with respect to the plate vector (Fig. 6.3). In contrast, uplifts or push-up blocks such as the Transverse Ranges, California and Lebanon Ranges, occur where the principal displacement zone is convergent with respect to the plate vector. This simple relationship is unlikely to apply where deformation takes place on many faults enclosing rotating crustal blocks. It is a very poor guide to patterns of uplift and subsidence in complex regions of continental convergence such as Turkey (Sengör et al. 1985).

Strike–slip zones are characterized by extreme structural complexity. Individual strike–slip faults are generally linear or curvilinear in plan view, steep (subvertical) in section and penetrate to considerable depths, perhaps decoupling crustal blocks at the base of the seismogenic crust (i.e., 10–15 km). In contrast to regions of pure extension or contraction, strike–slip zones possess promi-

nent *en echelon* faults and folds, and faults with normal and reverse slip commonly coexist. The vergence direction of folds and the mass transport indicators from thrusts associated with transpression are distinctively poorly clustered or apparently random.

Zones of major strike–slip tectonics are marked by important seismicity (Fig. 6.4). In California, the relative velocity between the Pacific and North American Plates is 47 mm yr^{-1}. Much of this displacement is taken up on the right-lateral (dextral) San Andreas Fault. However, like many other major translithospheric strike–slip faults, the San Andreas Fault occurs within a broader zone of faulting that may stretch laterally for 500 km. Much of the present day seismicity in the San Andreas system originates from faults oblique to the main fault zone (e.g., the NE-trending Garlock Fault and Big Pine Fault) (Nicholson et al. 1986). These oblique faults define crustal blocks that are rotating about a vertical axis. Seismicity dies out below about 15 km, indicating the brittle–ductile transition. Focal mechanism solutions in strike–slip zones are commonly highly variable, with mixtures of strike–slip, extension, and compression (e.g., North Anatolian Fault, Turkey, Taymaz et al. 1991), reflecting the complexities of deformation within a zone of overall strike–slip deformation.

Paleomagnetic studies support the idea that crustal blocks commonly undergo rotations about vertical axes (Fig. 6.5). The amount and scale of rotation varies greatly. The Western Transverse Ranges of southern California have experienced net clockwise rotations of 30°–90° for example, whereas in the Cajon Pass region there has been no significant rotation since 9.5 Ma. Small blocks can rotate rapidly, such as the Imperial Valley area, which has rotated by 35° in the last 0.9 Ma! The existence of such rotating blocks supports the view that the crustal blocks deform like a set of dominoes (Freund 1970). There is an obvious physical implication of the existence of rotating blocks, which is that the blocks must detach on their boundary faults at some level in the crust or upper mantle (Terres and Sylvester 1981; Dewey and Pindell 1985).

Pure strike–slip plate boundary faults should fall along a small circle drawn from the pole of rotation that defines the relative motion between the two plates. This is true for the San Andreas system along the boundary of the Pacific and North American Plates (Fig. 6.4). However, seismicity is distributed unevenly along the fault. In some regions there are very few historical earthquakes. The fault in these "locked" regions appears to accumulate strain and then release it in major earthquakes. The 1906 San Francisco moment magnitude 7.6 earthquake is an example. It produced a 4 m surface rupture all the way along a 200 km-long locked section from Redwood City to Cape Mendocino (Fig. 6.4). Elsewhere, small earthquakes are very abundant. In these "free" sections, frequent small earthquakes and aseismic creep release the accumulating strain.

The heat flow measured above major strike–slip faults, such as those of the San Andreas system, is low (Fig. 6.6) (Lachenbruch and Sass 1980, 1988). The heat flow associated with the Dead Sea transform is comparable to average continental values (Ben-Avraham et al. 1978). When slip on a fault occurs under a large stress, as given by Byerlee's law, significant frictional heating takes place. Repeated movements on a frictional strike–slip fault should generate large amounts of heat and contribute to elevated heat flows (Molnar 1992). The fact that observed heat flows are low suggests that major strike–slip faults are relatively weak structures set in a background of strong upper crust. Measurements of the principal stresses close to strike–slip faults in California also suggest that there is little shear stress resisting strike–slip fault motion (Zoback et al. 1987). Low heat flows also indicate that the localized extension along strike–slip zones does not in general involve significant mantle upwelling.

Whereas most of California has low to moderate surface heat flows, the Salton Trough–Imperial Valley in the extreme south has high surface heat flows (>2.5 HFU, Lachenbruch and Sass 1980) and known geothermal resource potential, as a northward continuation of the Gulf of California tectonic-thermal system (Figs. 6.6, 6.7). The region is active seismically, with right-lateral slip on the main Imperial Valley Fault. A seismic refraction and gravity study of the region (Fuis et al. 1984) shows that the Imperial Valley is a gravity high, despite the

Fig. 6.4 The San Andreas system, California. (a) Distribution of seismicity (stars). Solid arrows are relative plate velocities; open arrows are stress directions from focal mechanism studies; (b) Surface trace of the locked and unlocked sections of the San Andreas Fault. Dashed lines are small circles to the pole of rotation for the motion of the Pacific Plate relative to the North American Plate. Compiled from Jennings et al. (1975), Nicholson et al. (1986), and Turcotte and Schubert (2002). Reproduced courtesy of Cambridge University Press.

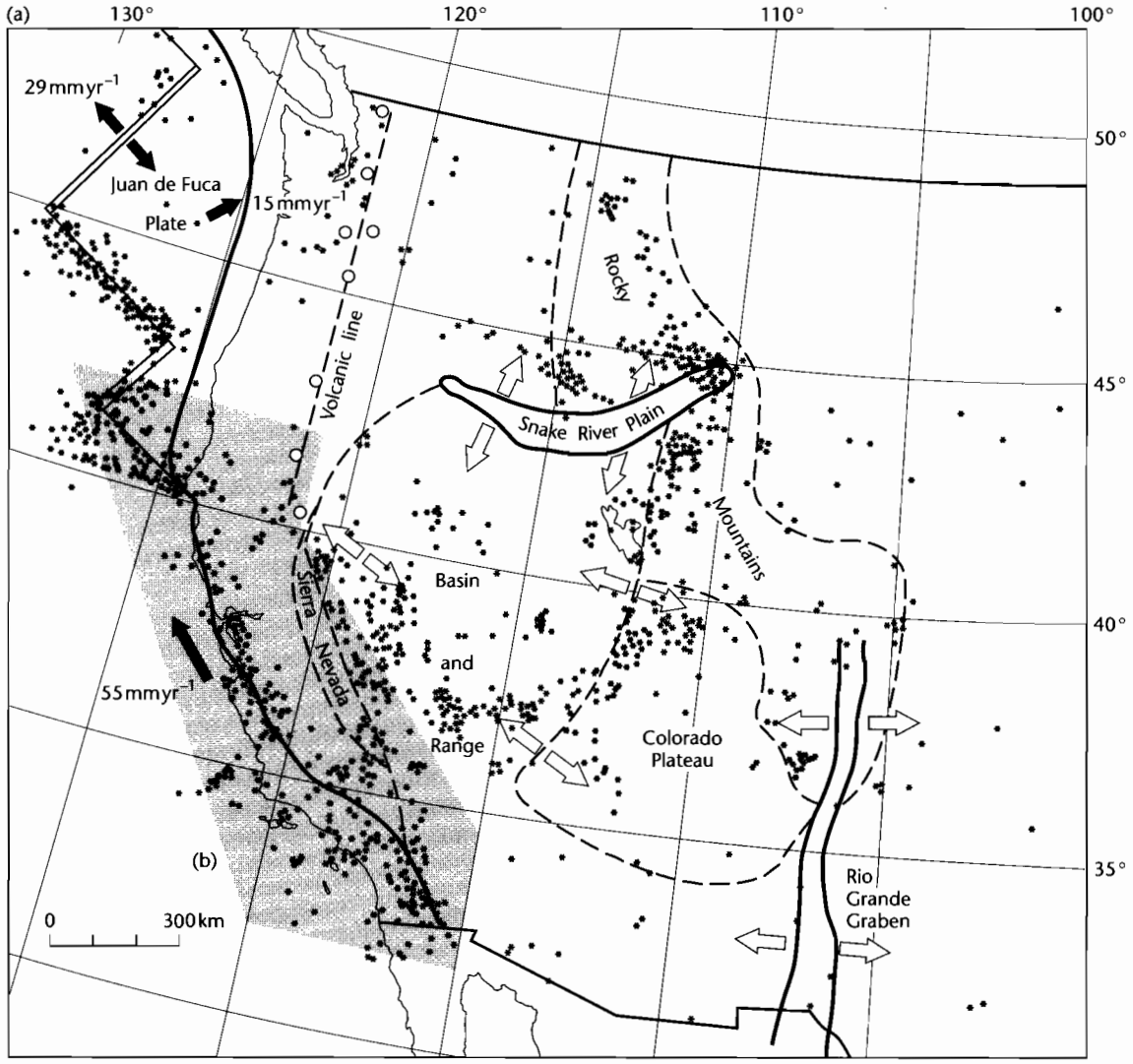
(a)
130°
120°
110°
100°
50°
45°
40°
35°
29 mm yr⁻¹
Juan de Fuca
Plate
15 mm yr⁻¹
Volcanic line
Rocky
Snake River Plain
Mountains
Basin
and
Range
Sierra Nevada
55 mm yr⁻¹
Colorado
Plateau
Rio
Grande
Graben
(b)
0
300 km

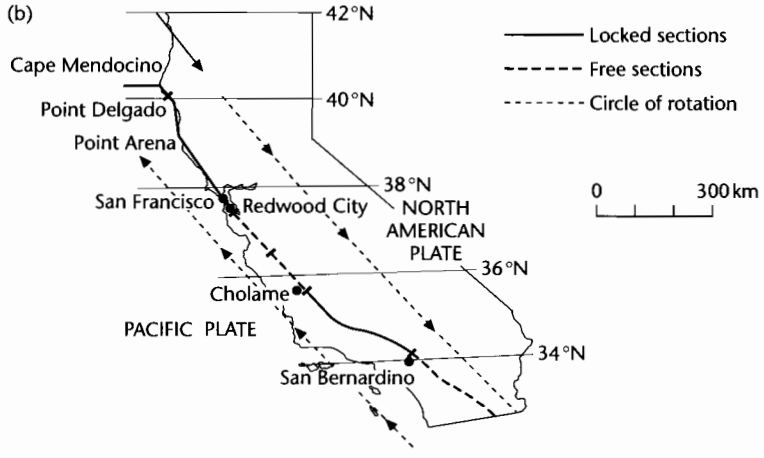
(b)
42°N
Cape Mendocino
40°N
Point Delgado
Point Arena
38°N
San Francisco
Redwood City
NORTH
AMERICAN
PLATE
36°N
Cholame
PACIFIC PLATE
34°N
San Bernardino
Locked sections
Free sections
Circle of rotation
0
300 km

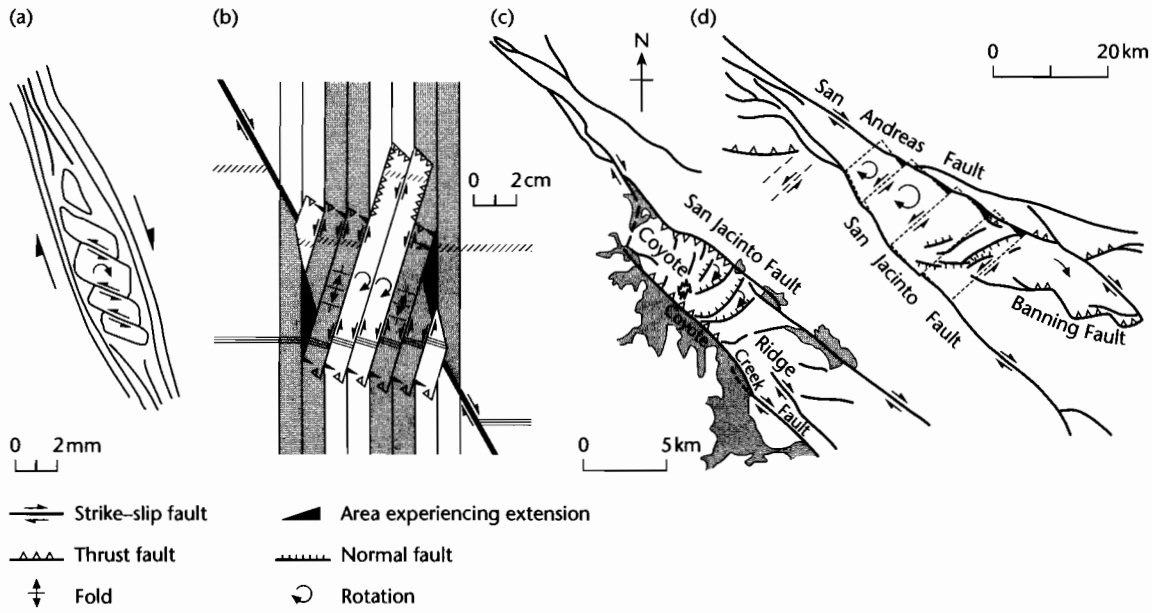

Fig. 6.5 Examples of block rotation by strike–slip faulting at scales from mm to km (after Nicholson et al. 1986). (a) Fracture and rotation of a felspar crystal along cleavage planes in a ductile matrix; (b) Rotation of a hard surface soil layer as a result of the Imperial Valley earthquake of 1979. The ruled lines are the evenly spaced furrows of a ploughed field; (c) Rotating blocks defined by secondary cross-faults between an overlapping right step from the Coyote Creek Fault to the San Jacinto Fault; (d) Block model for rotation near the intersection of the San Jacinto and San Andreas Faults inferred from geology and seismicity. Reproduced courtesy of American Geophysical Union.

presence of a 3.7–3.8 km thick sedimentary basin (Fig. 6.7). This is most likely due to the presence of intruded mafic basement domed up under the Imperial Valley where the extension is greatest.

Some of the world's best known and most hazardous faults, such as the San Andreas and North Anatolian Faults, are of the strike–slip variety. They commonly have startling geomorphic expression and stand out strongly in satellite images. The accumulation of individual slip events over long periods of time commonly results in a linear trough along the fault zone. Streams draining adjacent uplands and their interfluves are commonly offset laterally, demonstrating long-term strike–slip displacement. Since alluvial fans accumulate downstream of the range front, their apices may also be displaced laterally, and stream channels on the fan surface may thus become beheaded. Geomorphic evidence for strike–slip tectonics is classically displayed along the San Andreas system of California (Wesson et al. 1975; Keller et al. 1982) and along the Hexi Corridor of north-central China (Li and Yang 1998) (Fig. 6.8).

The evolution of some orogenic belts, notably the North American Cordillera, involves very large magnitude lateral displacements of terranes. Up to 1500 km of relative lateral motion is thought to have occurred in both the Mesozoic North American Cordillera and in the Tertiary India–Asia collision (Molnar and Tapponnier 1975). Clearly, strike–slip processes offer the possibility of immense lateral translations of crustal terranes.

6.1.2 Diversity of basins in strike–slip zones

Since the history of deformation is invariably complex in strike–slip zones, the associated sedimentary basins are correspondingly complex. They commonly form in areas of localized extension caused by the geometry and

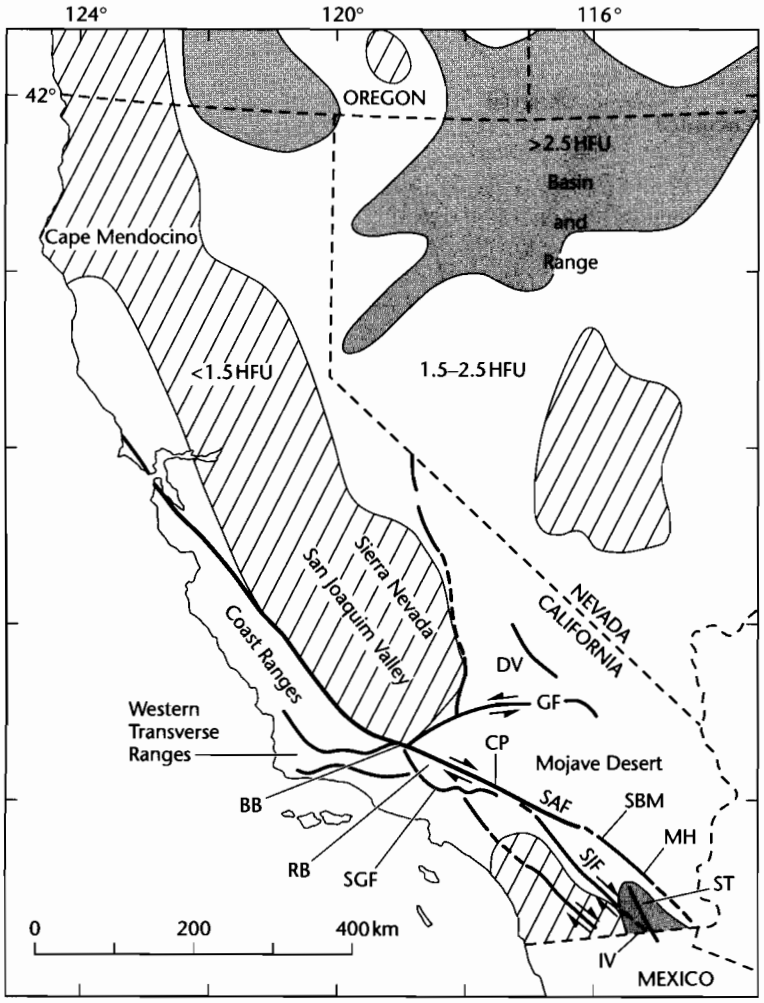

Fig. 6.6 Fault systems and heat flow provinces of California and adjacent regions (after Lachenbruch and Sass 1980). High heat flows are found in the extensional Basin and Range province and in the Salton Trough–Imperial Valley area close to the Mexican border. However, coastal California and most of southern California have low heat flows despite the presence of major strike–slip faults. BB, Big Bend; CP, Cajon Pass; DV, Death Valley; GF, Garlock Fault; IV, Imperial Valley; MH, Mecca Hills; RB, Ridge Basin; SAF, San Andreas Fault; SBM, San Bernardino Mountains; SGF, San Gabriel Fault; SJF, San Jacinto Fault; ST, Salton Trough.

kinematic history of the fault configuration, or in areas of net shortening, where flexural loading may drive subsidence. Characteristically, a basin experiences both extension and shortening during its life span (part of what Ingersoll (1988) calls the Reading cycle, after Reading (1980)), or one part of the basin may experience shortening while another part is undergoing extension.

Rift basins and foreland basins may undergo a phase of strike–slip deformation due to changes in the stress field set up by relative plate motion. Strike–slip basins are therefore emphatically syntectonic and there is little evidence of substantial thermally driven subsidence. This latter feature may be due at least in part to the small size of strike–slip basins. Their narrowness (usually less than

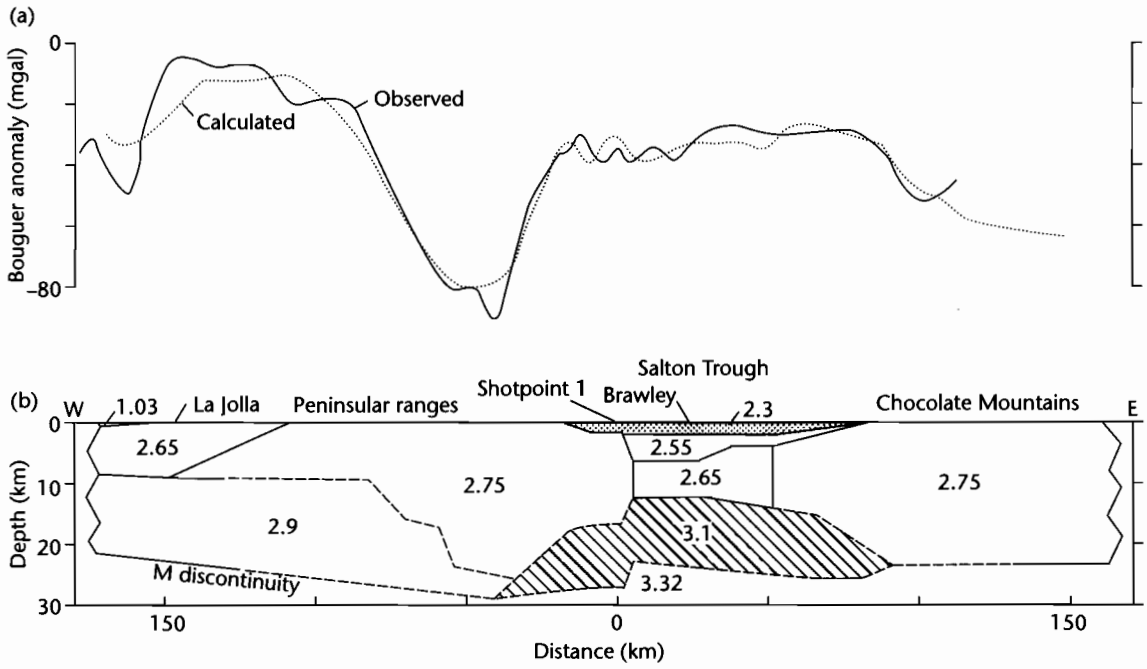

Fig. 6.7 Salton Trough–Imperial Valley region, southern California (after Fuis et al. 1982). (a) Gravity profile and (b) density model for a ENE cross-section of Imperial Valley from La Jolla to Chocolate Mountains. Solid lines on density model are derived from seismic refraction, whereas those that satisfy gravity data are shown dashed. A dense volume of sub-basement compensates gravitationally for the sedimentary rocks of the Salton Trough. Reproduced courtesy of United States Geological Survey.

50 km wide) causes extreme heat loss to the sides as well as vertical conduction to the overlying sea or atmosphere (§6.3.4).

A number of different types of basins form in strike–slip zones. General terms for these varied basins are "pull-apart basins" (Burchfiel and Stewart 1966) and "strike–slip basins" (Mann et al. 1983). The term "pull-apart basin" is also used for a subclass of basins formed in local transtensional settings (Ingersoll and Busby 1995).

We can identify two broad types of strike–slip basin in terms of thermal and subsidence history: (i) strike–slip basins with mantle involvement; these can be thought of as "hot" basins, and (ii) strike–slip basins that are relatively thin-skinned; they can be regarded as "cold" basins (Fig. 6.9).

A more detailed breakdown of basins in strike–slip zones on the basis of the kinematic setting and geometry of bounding faults has also been proposed. The advantage of such a scheme is that individual phases of basin evolution can potentially be discriminated, but the disadvantage is that many basins show characteristics of more than one type. A slightly modified version of the scheme proposed by Nilsen and Sylvester (1995) is as follows:

1 *Fault bend basins* commonly develop at bends in the main strike–slip fault where localized extension takes place. A type example is the Ridge Basin, California in the San Andreas system. The Vienna Basin, Austria is another basin developed at a releasing bend, but within a compressional orogenic setting;
2 *overstep basins* form between the ends of two subparallel strike–slip fault segments, which may merge at depth into one single master fault. A type example is the Dead Sea Basin along the Gulf of Aqaba–Dead Sea Transform, Middle East;
3 *transrotational basins* form as triangular gaps between crustal blocks undergoing rotation about a subvertical

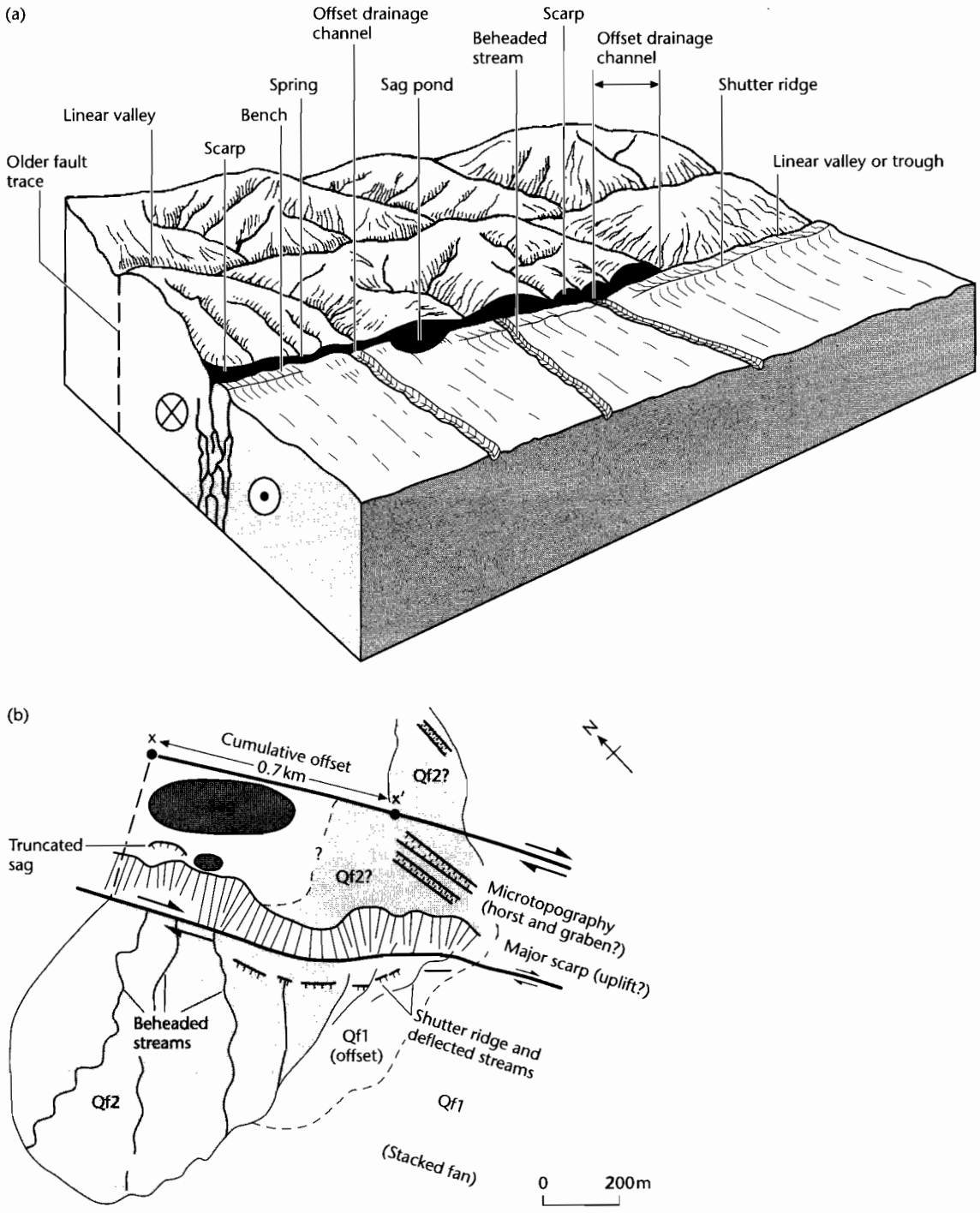

Fig. 6.8 Geomorphic features associated with strike–slip faults in the San Andreas system of California. (a) A linear trough along the fault, sag ponds, shutter ridges, offset ridges, and drainages, springs, scarps, and beheaded streams are typical geomorphic features indicative of strike–slip faulting. The older, abandoned fault trace displays analogous but erosionally degraded features. Modified from Wesson et al. (1975); (b) A large fan is offset from its catchment system, producing beheaded streams, shutter ridges, and extensional fault scarps. Modified from Keller et al. (1982). Reproduced courtesy of Blackwell Publishing Ltd.

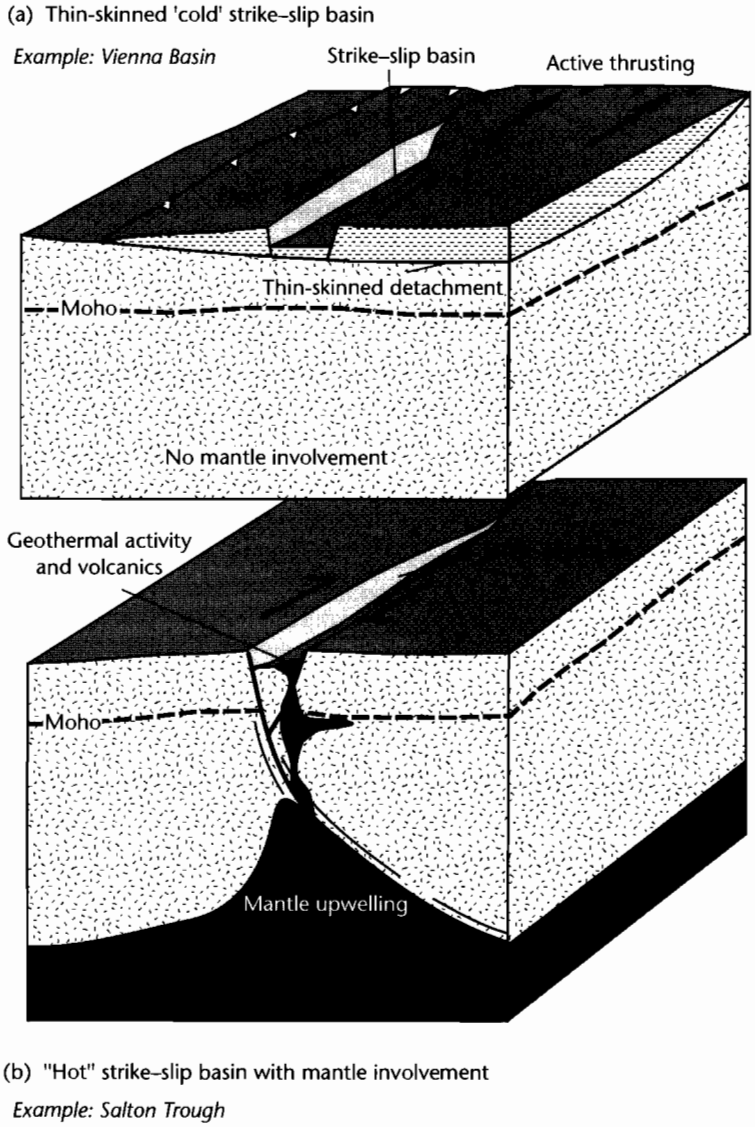

Fig. 6.9 Schematic diagram of broad classes of strike–slip basins. (a) Thin-skinned strike–slip basins, which are hypothermal; (b) Strike–slip basins with mantle involvement, which are hyperthermal.

axis. A type example is the Los Angeles Basin of southern California;

4 *transpressional basins* are elongate depressions parallel to the regional strike of folds and faults in zones of oblique convergence. These basins subside primarily by flexure caused by the supracrustal loads of compressional welts along the strike–slip zone. A type example is the Ventura Basin of California.

The sedimentary fill of strike–slip basins reflects their varied structural history, with highly asymmetrical longitudinal and transverse distribution of facies and abundant and complex unconformities. Subsidence rates

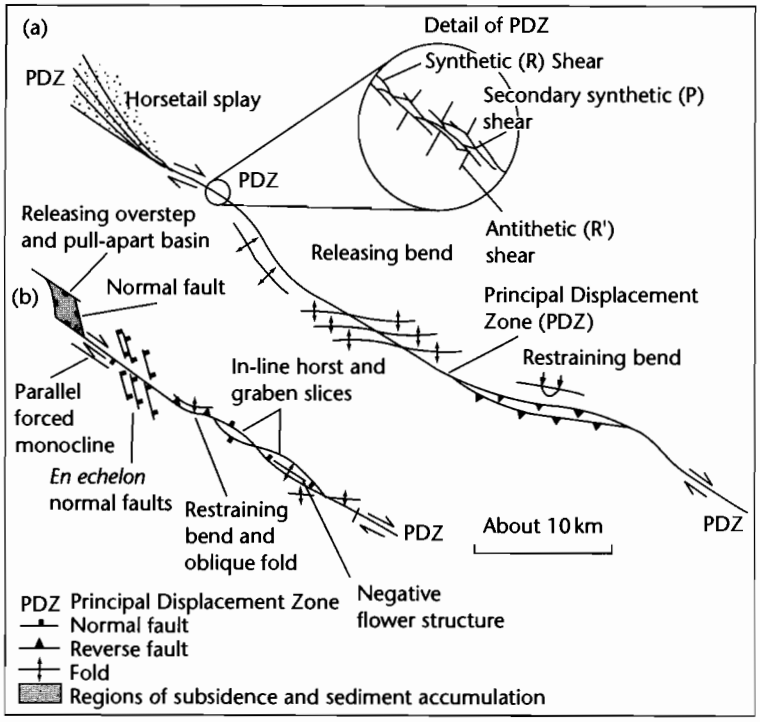

Fig. 6.10 (a) The plan view arrangement of structures associated with an idealized right-lateral (dextral) strike–slip fault; (b) Adaptation to a slightly divergent setting with the predominance of pull-aparts, *en echelon* normal faults, and graben slices within the PDZ.

are commonly extremely high, but subsidence may be relatively short-lived.

6.2 THE STRUCTURAL PATTERN OF STRIKE–SLIP FAULT SYSTEMS

6.2.1 Structural features of the principal displacement zone (PDZ)

Strike–slip faults are linear to curvilinear in plan view and generally possess a principal displacement zone (PDZ) along which the bulk of the shear strain is accommodated. However, changes in the orientation of the fault and/or the influences of the local geological fabric may cause deformation to extend beyond the PDZ into juxtaposed crustal blocks (Fig. 6.10). In cross-section, the principal displacement zones of large strike–slip faults are steeply inclined and commonly grade upwards from narrow, well-defined zones cutting igneous and metamorphic basement rocks at depth, to a braided, more diffuse deformation in the overlying sedimentary cover. This upward branching effect has led to the fault splays being christened "*flower structures*" or "*palm tree structures*" (Fig. 6.11). Some strike–slip faults link at depth with low-angle detachments, as occurs in foreland fold and thrust belts such as the Vienna Basin (Royden 1985) and in regions of regional extension such as the Basin and Range, USA (Cheadle et al. 1985). In the latter case, the Garlock Fault, a major strike–slip fault at a high angle to the San Andreas trend in California (Figs. 6.4, 6.6), appears to terminate downwards on a low angle surface situated in the middle crust (9–21 km depth) according to deep seismic reflection profiling (COCORP).

Figure 6.10 shows *en echelon* arrangements of faults and folds associated with strike–slip displacements. These structures are consistently arranged both in orientation and sense of strain with respect to the PDZ. They are

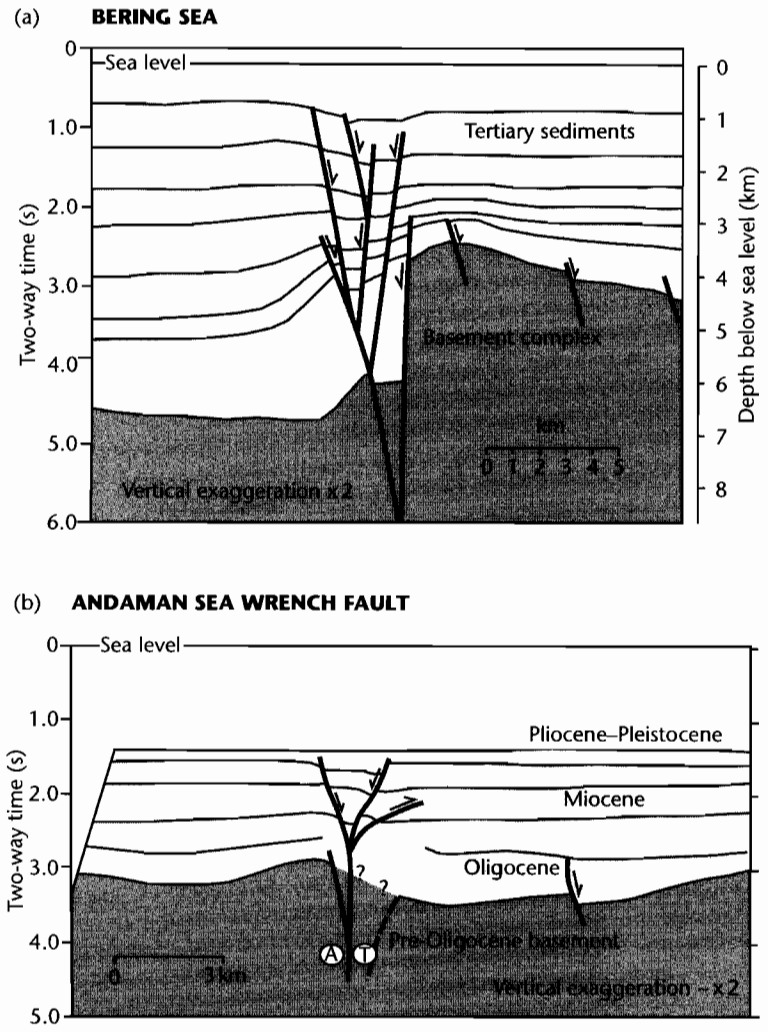

Fig. 6.11 The major characteristics in cross-sectional view of an idealized strike–slip fault. (a) Major fault zone in Bering Sea, (b) Andaman Sea wrench fault. Modified from Christie-Blick and Biddle (1985). A, displacement away from reader; T, displacement towards reader.

distinct from the *oversteps* between different segments of the principal displacement zone (§6.2.2). *En echelon* arrangements have been produced in model studies involving the deformation of clay, loose sand, or artificial materials (e.g., Riedel 1929; Cloos 1955; Harris and Cobbold 1984). Similar patterns have been observed in "natural" environments where alluvium has been affected by seismic disturbance, as in the 1975 earthquake in Imperial Valley, California (Sharp 1976). These experimental results and limited natural occurrences suggest that five sets of fractures are associated with a shear displacement (Fig. 6.12):

1 Synthetic strike–slip faults orientated at small angles to the regional shear couple. These are frequently termed *Riedel (R) shears*. The sense of offset is the same as that of the PDZ;
2 antithetic strike–slip faults orientated at high angles to the regional shear couple. These are termed *conjugate*

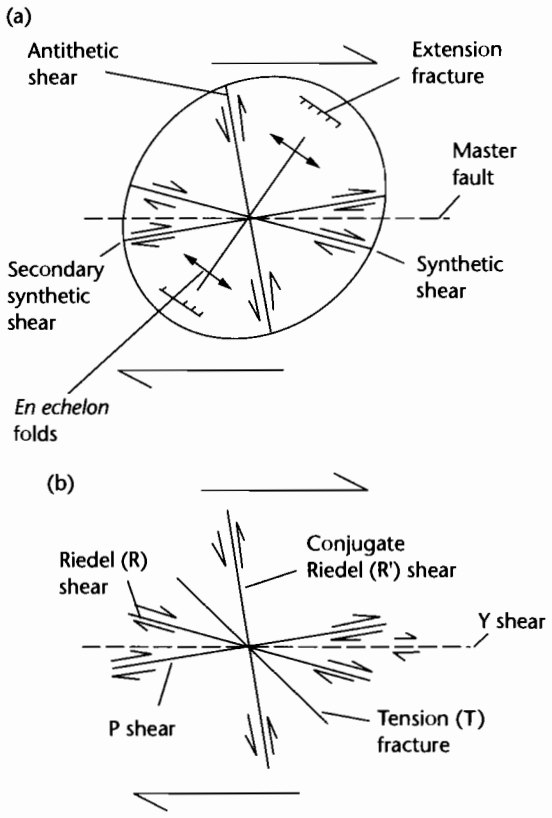

Fig. 6.12 The angular relations between structures that form in an idealized right-lateral simple shear, compiled from clay models and from geological examples (after Christie-Blick and Biddle 1985). (a) Fractures and folds superimposed on a strain ellipse for the overall deformation. Terminology of structures from Wilcox et al. (1973); (b) Riedel shear terminology modified from Tchalenko and Ambraseys (1970) and Bartlett et al. (1981).

Riedel shears or *R'*. The sense of offset is opposite to that of the PDZ;

3 secondary synthetic faults or *P-shears* with a sense of offset similar to that of the PDZ;
4 *tension fractures* related to extension in the strain ellipse;
5 faults parallel to the principal displacement zone and shear couple, or *Y-shears* of Bartlett et al. (1981).

En echelon folds develop with their axial traces parallel to the long axis of the strain ellipse, indicating shortening perpendicular to the extension demonstrated by the tension fractures (Fig. 6.12). Geological examples are invariably more complicated than the situation shown in figure 6.12, because the geological fabric influences fault orientations and also because faults and folds become rotated during progressive deformation so that the present fault configuration represents a cumulative picture over time. However, the idealized pattern is useful as a predictor of fault and fold occurrences if the regional shear direction is known, or, alternatively as a predictor of the latter where observations are possible on the resultant fracture and fold pattern.

The offset pattern on strike–slip faults in cross-section can be exceedingly complex. The sense of displacement may vary along one fault from horizon to horizon, and within a flower structure faults of opposite displacement occur together (Fig. 6.11). Additionally, a given fault in one cross-section may commonly switch in dip in another cross-section. These characteristics make strike–slip fault zones distinctive compared to regional extensional and contractional fault systems.

The precise structural pattern is controlled by a number of factors including (Christie-Blick and Biddle 1985): (i) convergent, divergent, or simple strike–slip (parallel) kinematics, (ii) magnitude of the displacement, (iii) material properties of the rocks and sedimentary infills in the deforming zone, and (iv) configuration of pre-existing structures giving a geological fabric.

(i) Convergent, divergent, and parallel kinematics

Convergent strike–slip causes the development of many reverse faults and *en echelon* folds. Depending on the obliquity of the strike–slip, this pattern may grade into a fold and thrust belt, as in the Western Transverse and Coast Ranges of California (Figs. 6.4, 6.6). Upward splaying flower structures have an overall antiformal structure caused by the net shortening. They are commonly known as *positive flower structures*. Folds are less well developed in divergent strike–slip settings, taking the form of flexures associated with extensional faulting. Flower structures take on an overall synformal structure in regions of net divergence, and are consequently known as *negative flower structures*. The Tekirdag Depression in the Marmara Sea, Turkey, situated along a restraining bend of the North Anatolian Fault, is situated in a broad negative flower structure (Okay et al. 1999) (Fig. 6.13).

The scale of the distribution of convergence or divergence varies from regional to local. For example, regional divergent strike–slip may take place where major fault

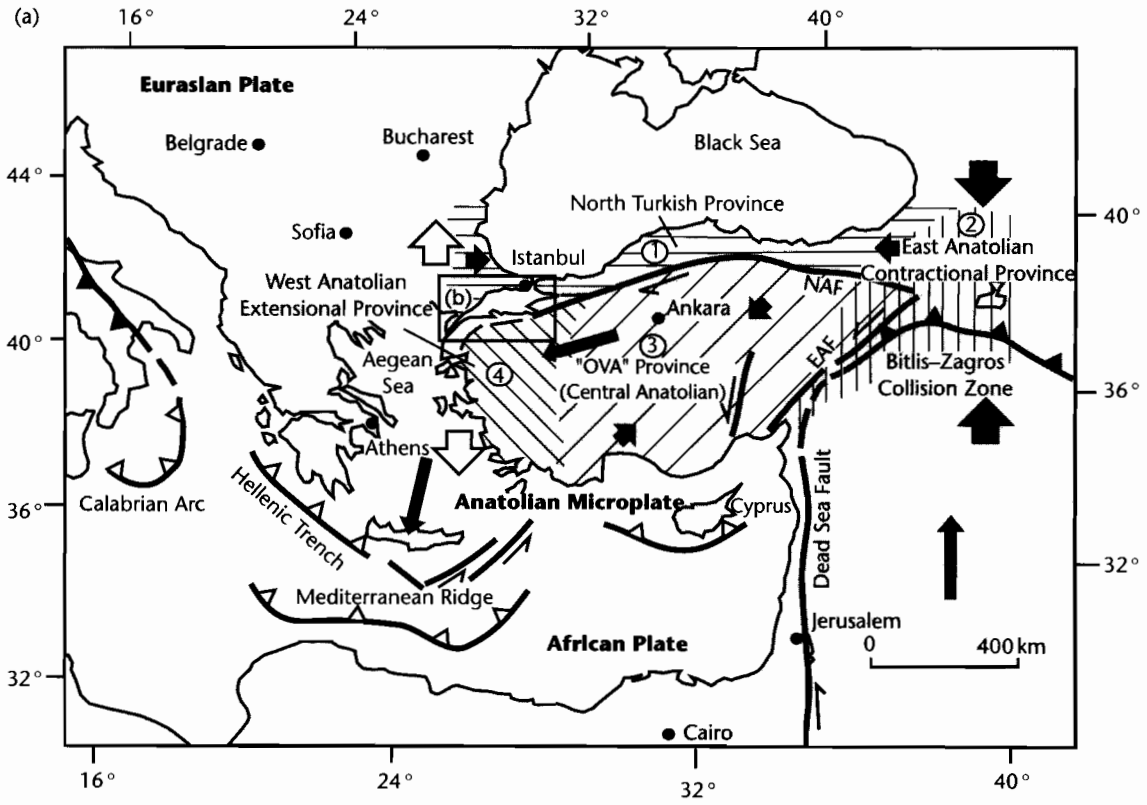
(a)
16°
24°
32°
40°
Eurasian Plate
Belgrade
Bucharest
Black Sea
44°
North Turkish Province
Sofia
Istanbul
East Anatolian
Contractional Province
West Anatolian
Extensional Province
(b)
NAF
Ankara
40°
Aegean
Sea
"OVA" Province
(Central Anatolian)
EAF
Bitlis–Zagros
Collision Zone
36°
Athens
Calabrian Arc
Hellenic Trench
Anatolian Microplate
Cyprus
Dead Sea Fault
32°
Mediterranean Ridge
Jerusalem
African Plate
0
400 km
Cairo
16°
24°
32°
40°

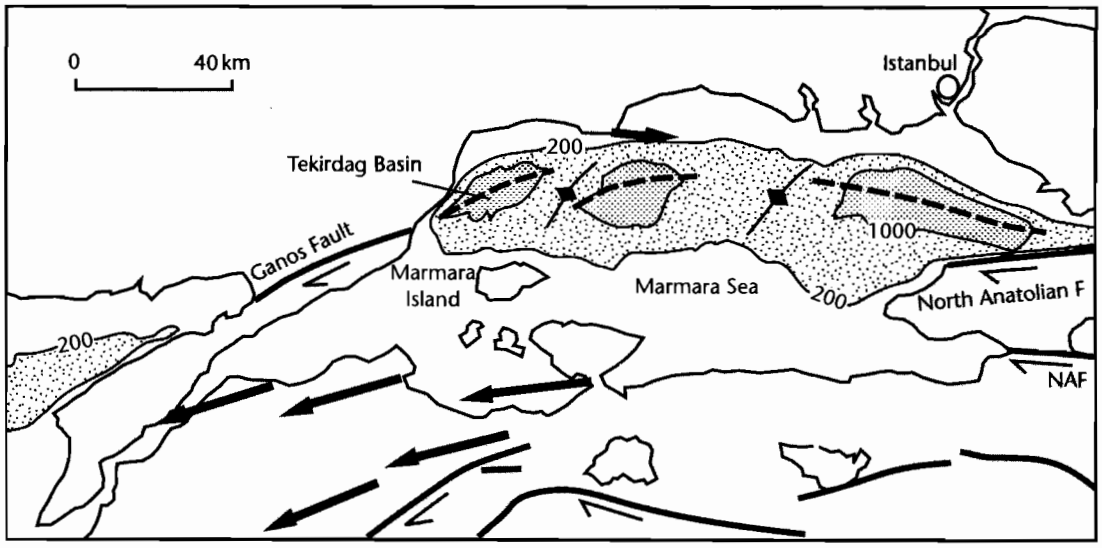
(b)
0
40 km
Istanbul
Tekirdag Basin
200
1000
Ganos Fault
Marmara
Island
Marmara Sea
200
North Anatolian F
200
NAF

strands are oblique to interplate slip vectors as in the Dead Sea Transform (Fig. 6.3). On a much more local scale, divergent strike–slip may take place at releasing fault oversteps and fault junctions. Divergent strike–slip faults also develop on a local scale where crustal blocks rotate between bounding wrench faults.

A detailed study of the rotations and oversteps associated with a strike–slip displacement following a recent earthquake was carried out by Terres and Sylvester (1981). The deformation of a recently ploughed carrot field in Imperial Valley following the earthquake of October 15, 1979 is shown in figure 6.5b. This very small-scale example shows many of the features predicted from model experiments with both extension and contraction occurring simultaneously. The topsoil broke up into elongate blocks along the furrows and these blocks moved relative to each other along conjugate Riedel shears (R') or antithetic shears. Extension occurred along the long axis of the strain ellipse and folding along the short axis. The elongate blocks delimited by shears, which Dewey (1982) has termed "*Riedel flakes*," show clockwise rotations in this example of right-lateral strike–slip. A much larger rotated block with dimensions of 20 km by 70 km, the Almacik flake along the North Anatolian Fault, Turkey, is also thought to be due to Riedel flaking (Sengör et al. 1985) (Fig. 6.14). Here, clockwise rotation of the tectonostratigraphic

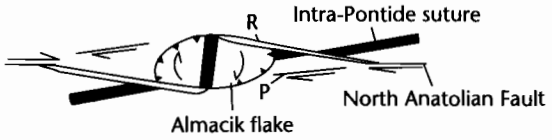

Fig. 6.14 Interpretation of the Almacik flake along the North Anatolian Fault in Turkey (Sengör et al. 1985), based on the idea of "Riedel flaking." R and P shears are shown.

domains of 110° has taken place since the initiation of faulting. The right-lateral strike–slip along the North Anatolian PDZ has produced families of thrusts, Riedel and P shears.

Rotations may also take place along straight segments of adjacent strike–slip faults, causing geometrical space problems. These space problems are resolved by gaps and overlaps occurring at fault block corners known as transrotational basins. Figure 6.15 (see also Fig. 6.5d) shows how regions of extension and contraction may alternate along the strike–slip fault.

(ii) Magnitude of the displacement

Laboratory experiments indicate that there is a sequential development of structural features in strike–slip zones (Tchalenko 1970 and Wilcox et al. 1973 for clay models, Bartlett et al. 1981 for rock samples under confining pressure). In the rock sample experiments, the zone of deformation first of all expands rapidly due to the development of folds and fractures. Weakening of the deforming zone soon, however, stabilizes the spread of the zone of deformation, and later structures are concentrated in a central core zone (Odonne and Vialon 1983). All early formed structures are rotated by later deformations, so their orientation is dependent on the magnitude of the displacement.

Some of the features observed in experiments can be found in natural occurrences, whereas other features are difficult to match. An increasing complexity from discontinuous faults and folds along low displacement boundaries to through-going PDZs along high displacement boundaries is commonly observed. Active fault systems that are accompanied by sedimentation may, however, be buried faster than they deform. In this way, the uppermost, younger sediments may record less deformation than the older stratigraphy.

Fig. 6.13 (a) Tectonics of the eastern Mediterranean. The four main tectonic regimes of Turkey (shown by numbers in circles) are caused by the post late Serravalian (*c.* 12 Ma) westward escape of the Anatolian block from the east Anatolian convergence zone onto the oceanic lithosphere of the eastern Mediterranean Sea (after Sengor et al. 1985). (1) Weakly active North Turkish province characterized by limited E–W shortening; (2) East Anatolian contractional province of N–S shortening, situated mostly to the east of the meeting point of the East Anatolian and North Anatolian strike–slip faults; (3) the Central Anatolian "Ova" province with NE–SW shortening and NW–SE extension, containing large, roughly equant-shaped complex basins termed "ovas"; (4) West Anatolian extensional province characterized by N–S extension. The arrows are roughly proportional to the magnitude of the total strain. EAF, East Anatolian Fault; NAF, North Anatolian Fault; (b) Detail of the Marmara Sea region along the North Anatolian Fault Zone (Okay et al. 1999), showing selected bathymetric contours. Fault plane solutions are from Taymaz et al. (1991). Arrows are displacement vectors derived from GPS using a fixed station at Istanbul (Straub and Kahle 1995). The Tekirdag Basin is located in a broad negative flower structure.

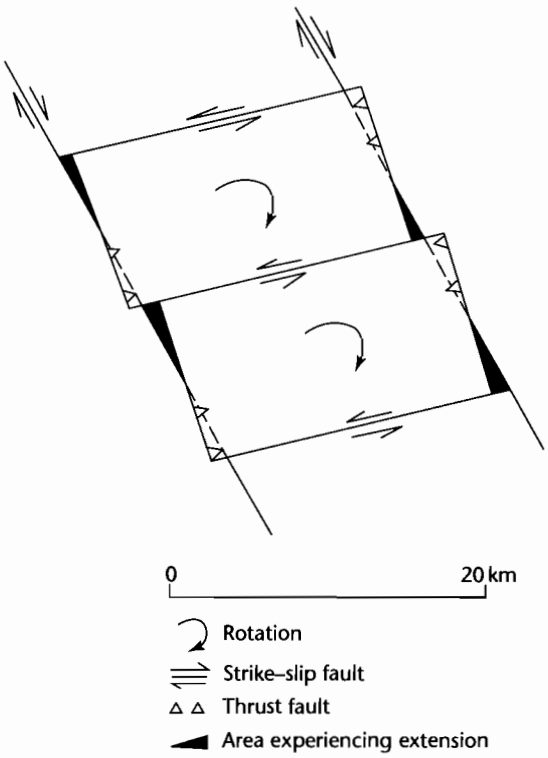

Fig. 6.15 Model of rotation of blocks near the intersection of the San Andreas and San Jacinto Faults, California, based on earthquake hypocentral locations and first motion studies (Dibblee 1977; Nicholson et al. 1985a, b). During a large earthquake, one of the bounding faults moves by right-lateral slip. Continued aseismic motion between the bounding faults is accommodated by clockwise rotations of small blocks and by minor left-lateral movements on faults defining these rotating blocks. Rotation causes overlaps (small reverse faults) and gaps (small normal faults) to form along the major bounding right-lateral faults. Viewed on a crustal scale, these rotating flakes would be detached from the underlying lower crust/mantle by thrust faults that would merge with the associated left-lateral strike–slip faults.

(iii) Material properties in the deforming zone

The lithologies of rocks in the strike–slip zone and the rates and pressure–temperature conditions of deformation all control the individual structural character of the fault zone. These factors vary from one strike–slip zone to another, but they also may vary in time within an individual strike–slip fault system. Deformation of different stratigraphic units, strain weakening, or strain hardening effects, uplift, and erosion or sedimentation and burial, or changes in heat flow related to crustal thinning and/or volcanism can all have significant effects on the evolution of the fault zone.

(iv) Pre-existing geological fabric

Continental strike–slip fault systems commonly intersect or make use of older heterogeneities. For example, the Great Basin, western USA underwent Laramide shortening (NE–SW trend), then two phases of extension, one related to backarc processes (axis of extension orientated NE–SW), the other to the development of a right-lateral megashear (change in extension direction to NW–SE). The right-lateral faults and, locally, conjugate left-lateral faults associated with this clockwise rotation in the extension direction may well be related to the existence of older crustal structures.

The Great Basin is an example of regional extension, so the strike–slip motion is taking place in a transtensile regime. The Rhine Graben of western Europe, however, originated in a background environment of continental collision north of the Alps in Late Eocene times. Early extensional faults in the Late Eocene–Oligocene were used as strike–slip faults in the Pliocene to Holocene (Illies 1977; Illies and Greiner 1978).

Pre-existing structures that significantly influence the location and orientation of folds and faults during strike–slip are termed "*essential*" structures. However, pre-existing structures that exert no control on later deformation are termed "*incidental*" (Christie-Blick and Biddle 1985, p.13).

6.2.2 Role of oversteps

In §6.1.2 the location of overstep basins between the tips of two subparallel strike–slip fault segments was introduced. An *overstep* or *stepover* is a structural discontinuity between two approximately parallel overlapping or underlapping faults. Oversteps are extremely important in determining the location of regions of subsidence and uplift along a strike–slip system. We consider a numerical model of basin development at an overstep in a later section (§6.3.3). There appear to be two basic types (Fig. 6.16):

- Oversteps along the strike of faults, that is, observed in plan view; faults are continuous in the down-dip direction;

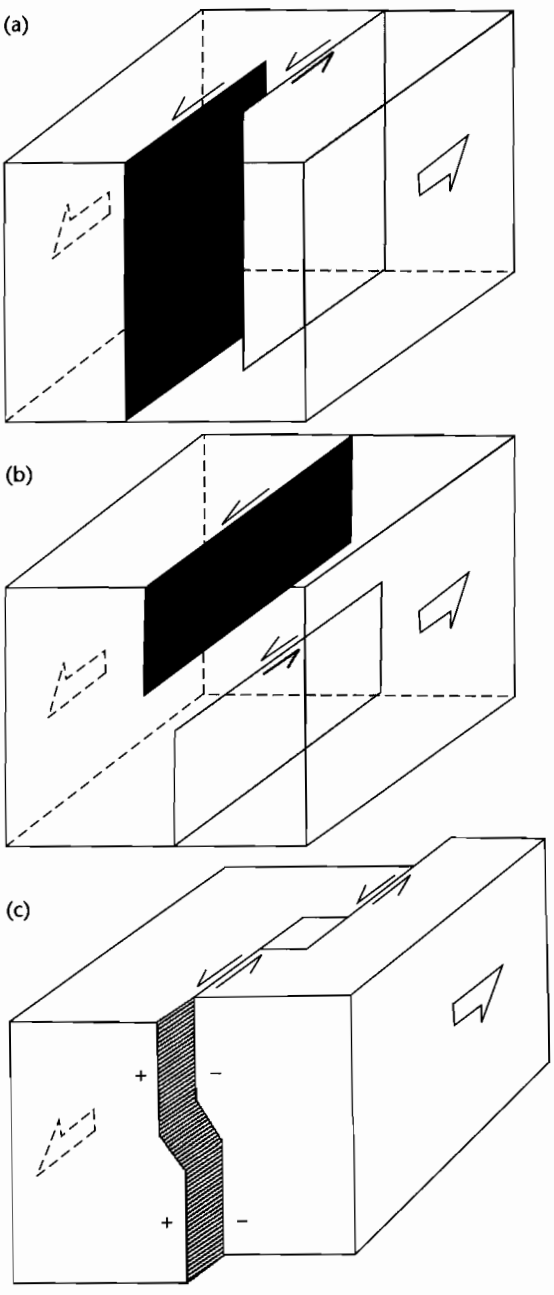

Fig. 6.16 Oversteps on strike–slip faults. (a) Along-strike oversteps in which faults are continuous in the down-dip direction; (b) Down-dip oversteps in which the faults are continuous in plan view; (c) Combination of along-strike and down-dip oversteps, with a pull-apart basin located at the along-strike overstep (after Aydin and Nur 1985).

- oversteps along the dip of faults, that is, observed in cross-section; faults are otherwise continuous in plan view.

Both types of overstep may occur along the same fault or fault zone. If the sense of an along-strike overstep is the same as the sense of fault slip, a *pull-apart basin* is formed (Aydin and Nur 1985). If, however, the sense of the overstep is opposite to that of fault slip, a *push-up range* is formed. Down-dip oversteps are probably as important as along-strike oversteps, but are more difficult to identify and map. Seismicity studies on active strike–slip faults such as the Calaveras Fault, California, show a distinct offset of the trends of hypocenters, breaking the fault into an upper segment (2–7 km depth) and a lower segment 2 km away (4–10 km depth). This suggests that a down-dip overstep is present (Reasenberg and Ellsworth 1982).

6.3 BASINS IN STRIKE–SLIP ZONES

In general, subsidence in strike–slip zones tends to occur where the deformation is accompanied by a component of divergence (Fig. 6.3), such as at bends and oversteps in the fault or in gaps between rotating flakes. Uplift, however, tends to occur where there is a component of convergence (Fig. 6.3), although flexure of an underlying block by an overriding block may cause subsidence. Uplift takes place at convergences of faults into a fault junction or at bends in fault traces. These zones of uplift provide sourcelands of detritus available to fill nearby basins. Bends, oversteps, and fault junctions associated predominantly with extension and subsidence are termed "*releasing*," whilst those associated with shortening and uplift are termed "*restraining*" (Crowell 1974). Parallel-sided basins in which oceanic crust occurs are termed *rhombo-chasms* (Carey 1976).

The causes of fault bends, oversteps, and junctions are varied. Some bends may result from pre-existing crustal heterogeneities, as in the case of strike–slip faults propagating along older extensional fractures. This appears to be the case in Jamaica (Mann et al. 1985), which lies entirely within a 200 km-wide seismic zone of left-lateral strike–slip deformation between the North American and Caribbean Plates. Extensional faults at the east of the Paleocene–Eocene Wagwater Rift Graben have been reactivated as reverse faults along a restraining bend in the Neogene strike–slip system. Other bends may be due to deformation of initially straight faults as a result of incompatible slip at a fault junction (e.g., the "big-bend"

of the San Andreas Fault, Figs. 6.4, 6.5), rotation of adjacent blocks (southern San Andreas Fault), or intersection of the fault with a zone of greater extensional strain (e.g., western end of North Anatolian Fault) or contractional strain (e.g., near junction of North Anatolian and East Anatolian Faults in eastern Turkey, Fig. 6.13).

Fault branching and oversteps may develop by a number of mechanisms including segmentation of curved fault traces, intersection of weak zones orientated obliquely to the direction of strike–slip and changes in stress fields caused by fault interaction. The precise reasons for the formation of oversteps and branches remains obscure (Aydin and Nur 1985).

Strike–slip basins may be *detached* and therefore thin-skinned. Examples are known from both areas of pronounced regional shortening such as the Vienna Basin and the St George Basin in the Bering Sea, Alaska, and in areas of regional extension such as the West Anatolian extensional province of Turkey and the Basin and Range of the USA.

6.3.1 Kinematic models for pull-apart basins

A number of kinematic models exist for the development of pull-apart basins (Fig. 6.17):

1 Overlap of side-stepping faults: The simplest model is based on pioneer field studies of active strike–slip basins such as the Dead Sea and the Hope Fault Zone in New Zealand. Discontinuous parallel fault segments which have a horizontal separation develop oversteps. As the master faults lengthen, producing more overlap, the basin lengthens while its width remains fixed by the original separation of the parallel master faults. This model has been widely applied to the San Andreas Fault system in the Gulf of California–Salton Trough area (Crowell 1974), and the Dead Sea Fault system (Garfunkel et al. 1981). This configuration of lengthening, parallel master faults has been used to simulate pull-apart development using elastic dislocation theory (Rodgers 1980) (see §6.3.3). This theory predicts that distinct changes occur in the strike–slip basin as the amount of overlap of the master faults increases. Specifically, when the overlap is about equal to the separation, the pull-apart develops two depocenters in regions of extension separated by a zone of secondary strike–slip faulting in the basement. As the overlap increases, the depocenters become more widely spaced and the intervening zone of strike–slip faulting broader. Although there are instances where field observations fit the theoretical elastic dislocation model rather well (e.g., Cariaco Basin, Venezuelan part of southern Caribbean, Schubert 1982), basins that are filled with sediment more rapidly than the upward propagation of faults from the basement may develop fault systems at strong variance to those predicted by elastic dislocation theory. The presence of two distinct depocenters associated with strain above each fault segment has rarely been observed.

2 Slip on divergent fault segments: Detailed field mapping of some active pull-aparts suggests that bounding strike–slip faults may be nonparallel (Freund 1971). If nonparallel, nonoverlapping faults are slightly divergent and connected by a short oblique segment, continued strike–slip may open up a basin along one side of the oblique fault and cause compression along the other side.

3 Nucleation on *en echelon* fractures or Riedel shears: Shear box experiments suggest that pull-apart basins may be structurally analogous to *en echelon* extensional fractures produced in clay materials. As deformation continues, the shear fractures join to form a pull-apart basin. A similar process of formation from rotated large scale tension gashes or Riedel shears has also been proposed.

4 Coalescence of adjacent pull-aparts into larger system: A worldwide compilation of the dimensions of a large number of pull-aparts suggests that there is a linear relation between the basin length (fault overlap) and the basin width (fault separation) (Aydin and Nur 1982). This scale dependence of pull-apart basins suggested that they are commonly three times as long as they are wide irrespective of their absolute size. This may be due to the coalescence of adjacent pull-aparts in a single larger basin with increasing offset, or to the formation of new fault strands parallel to existing ones.

5 Transform-normal extension: Markedly asymmetric, large strike–slip basins bounded by a transform segment on one side and subparallel normal faults on the other, may be due to transform–normal extension (Ben-Avraham and Zoback 1992). Examples of highly asymmetric basins are the Gulf of Elat (Dead Sea Transform) (Ben-Avraham 1985) and the Cariaco Basin (offshore Venezuela). In the Gulf of Elat (Fig. 6.18), the sense of asymmetry switches along the PDZ, the deeper side of

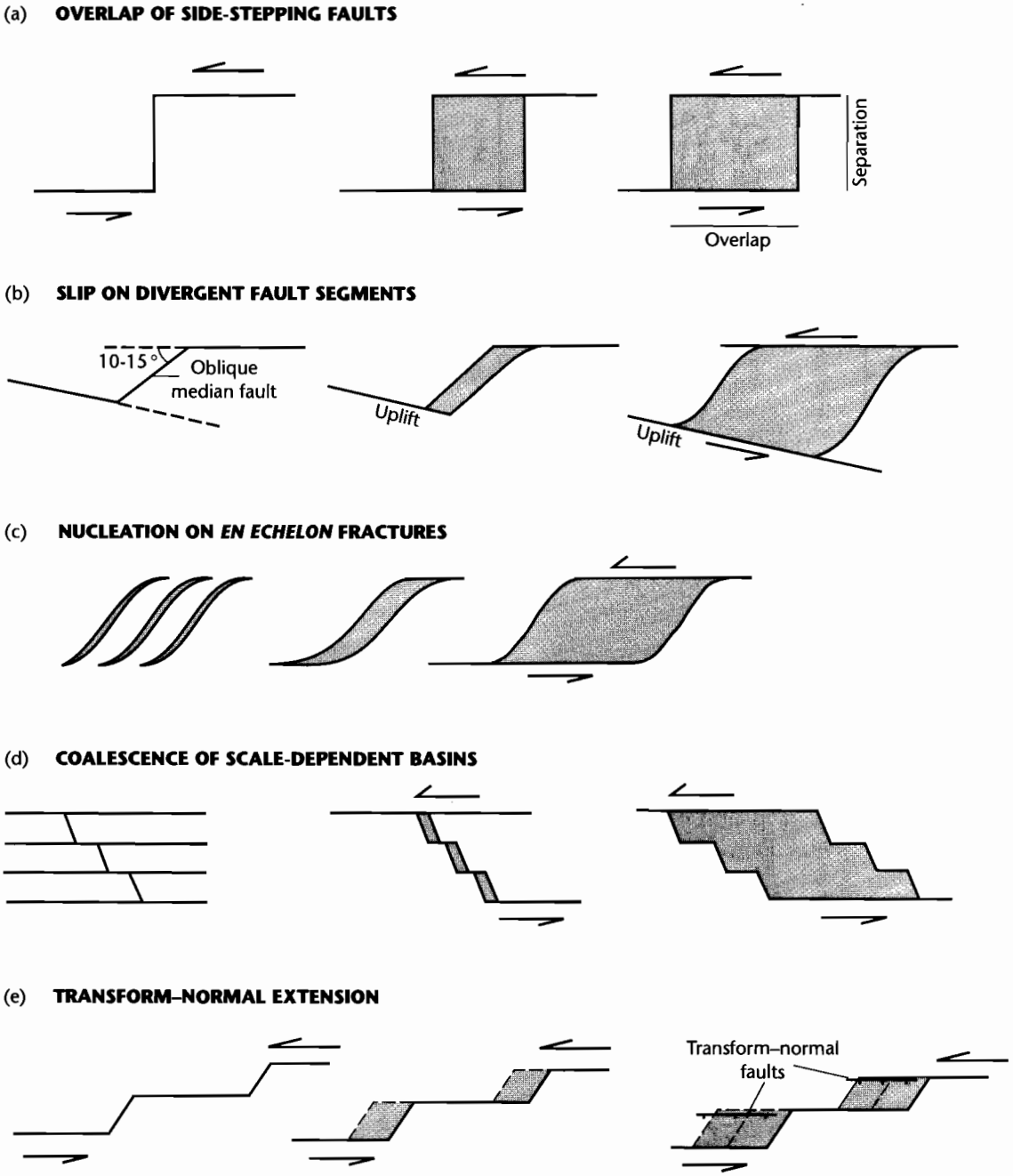

Fig. 6.17 Models of pull-apart basin development (after Mann et al. 1983, and Ben-Avraham and Zoback 1992). (a) Pull-apart opening between left-stepping and sinistral master strike–slip faults. Fault separation and basin width remain constant through time whereas fault overlap and basin length increase with the amount of strike–slip displacement. The elastic dislocation model of Rodgers (1980) applies to this kind of pull-apart mechanism; (b) Pull-apart opening across an oblique median fault and nonparallel master faults. Note that compression and uplift occur on one side of the pull-apart while an extensional "gap" develops on the other; (c) Pull-apart formation by nucleation from extensional fractures, based on shear box experiments (Koide and Bhattacharji 1977); (d) Pull-apart formation by coalescence of small scale-similar sub-basins, as suggested by Aydin and Nur (1982). This allows the widening of pull-aparts with increased offset, in contrast to (a); (e) Pull-apart basin formation caused by simultaneous strike–slip motion on a transform fault and transform–normal extension (after Ben-Avraham and Zoback 1992). The pull-aparts are markedly asymmetric towards the transform fault.

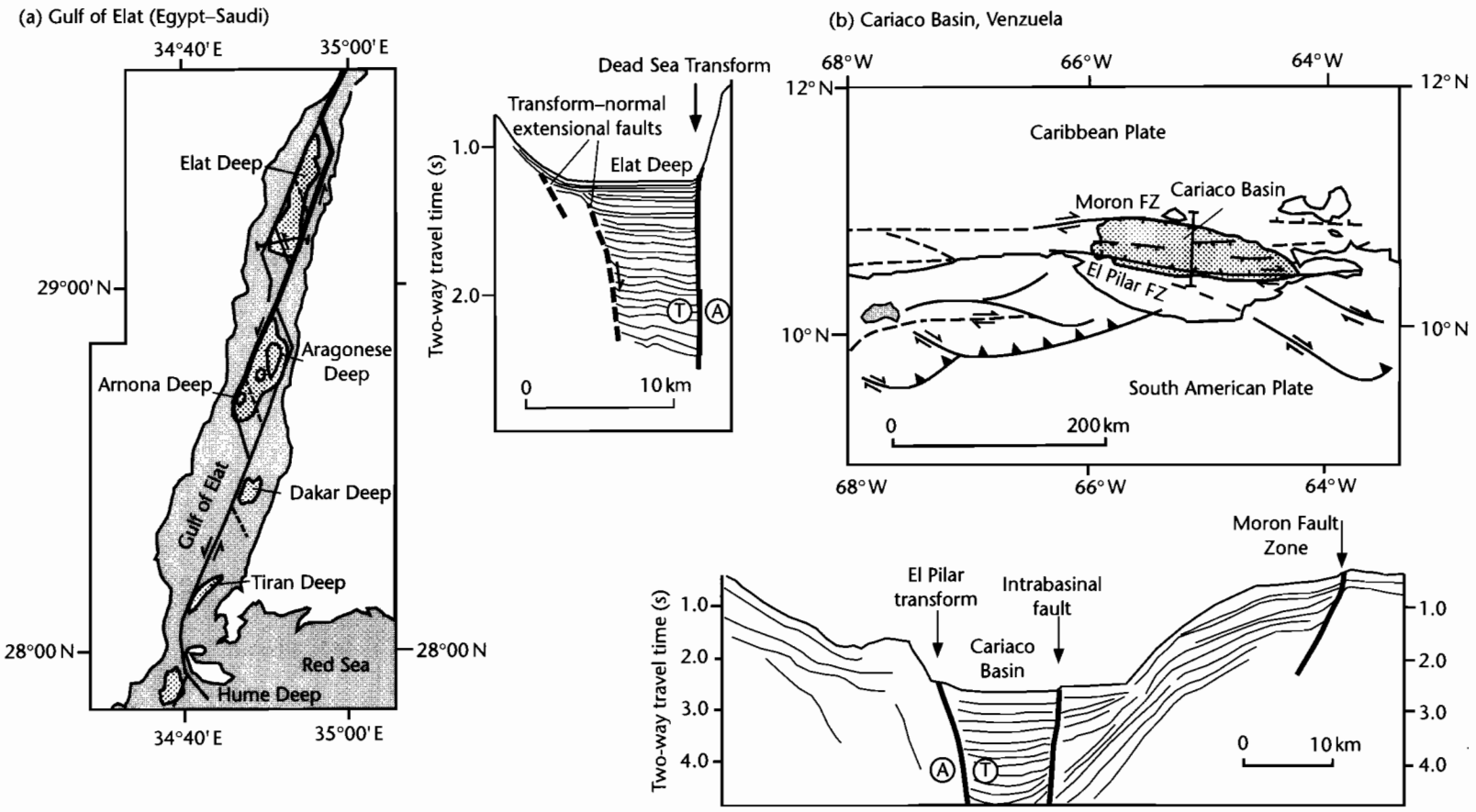

Fig. 6.18 (a) Bathymetry and structure of the Gulf of Elat showing segments of the Dead Sea Transform and location of main topographic depressions. Inset shows cross-sectional geometry across the Elat Deep derived from seismic reflection surveys. Asymmetry of the basin-fill is towards the transform fault; (b) Tectonic map and seismic profile across Cariaco Basin, northern Venezuela (Schubert 1982), showing basin asymmetry towards El Pilar Transform. A, displacement away from reader; T, displacement toward reader. Modified from Ben-Avraham and Zoback (1992).

the sub-basin always being located against the strike–slip Dead Sea Transform, with the shallower flank adjacent to normal faults. This suggests that subsidence occurs due to extension approximately normal to the transform at the same time as strike–slip displacement is taking place, in contrast with kinematic models of deformation in strike–slip zones where extension and compression directions are at 30–45° to the strike–slip fault plane (Fig. 6.12). This style of deformation may be due to the weakness of strike–slip faults (see also §6.3.3). A model of stress orientation close to weak transform faults embedded in a strong crust (Zoback et al. 1987) suggests that far-field transtensional stresses cause fault-normal extension, and transpressional stresses cause fault-normal compression.

6.3.2 Continuum development from a releasing bend: evolutionary sequence of a pull-apart basin

Analysis of neotectonic pull-apart basins in their embryonic stage suggests that they are associated with: (i) releasing bend geometries, in which master faults do not overlap but are connected by oblique median strike–slip faults, and (ii) nonparallel master faults (see also (1) and (2) above). Gentle restraining bends appear to produce narrow *spindle-shaped* pull-aparts like the Clonard Basin, Haiti at the left-step in the Enriquillo–Plantain Garden Fault Zone. In contrast, sharp restraining bends produce multiple, staggered pull-aparts as in the Salton Trough of California. Since embryonic pull-aparts appear to occur on releasing bends of through-going faults, they are unlikely to be analogous to the tension gashes or Riedel shears produced in shear box experiments (see (3) above).

Continued offset produces basin shapes known as "*lazy S*" (between sinistral faults) and "*lazy Z*" (between dextral faults) (Mann et al. 1983) (Fig. 6.19), representing a transitional stage between spindle-shaped basins between master faults with no overlap and rhomboidal basins between overlapping master faults. S- and Z-shaped pull-aparts are particularly common where the master faults are widely separated (>10 km) and their strikes are nonparallel. The Death Valley Basin, California has a pronounced Z-shape.

Lengthening of the S- or Z-shaped basins produces rhomb-shaped pull-aparts. Length to width ratios (overlap to separation) increase by this process because the separation remains fixed by the width of the releasing bend. Rhomboidal pull aparts are characterized by overlapping master faults and deep depocentres at the ends of the pull apart basin, separated by a shallow sill(s). The Cariaco Basin of the Venezuelan Borderlands is a good example, with two subcircular deeps in excess of 1400 m and a shallow sill at 900 m. Multiple deeps may be arranged diagonally across the rhomboidal pull-apart, as is the case in the Gulf of Aqaba in the northern Red Sea, the deepest segment of the sinistral Dead Sea Fault System (Ben-Avraham et al. 1979). The rapid subsidence between the overlapping master faults generally greatly exceeds sedimentation, leading to deep marine or lacustrine environments. The presence of prominent depocenters at the ends of rhomboidal pull-aparts does not support the mechanism of simple extension between overlapped master faults (see (1) above), but is predicted by the elastic dislocation model (Rodgers 1980). An alternative view is that the depocenters may in fact be smaller pull-aparts in the basin floor of the larger pull-apart, that is, the rhomboidal basin is in a coalesced stage of development (see (4) above).

With continued offset, rhomboidal pull aparts may develop into narrow oceanic basins where the length (overlap) greatly exceeds the basin width (separation). The Cayman Trough along the boundary between the Caribbean and North American Plates is a type example. The large length/width ratio suggests that coalescence is unimportant at this stage.

6.3.3 Numerical modeling of pull-apart basins

A number of quantitative approaches are possible to the formation of basins in strike–slip zones, involving a basal shear driving displacement on faults cutting the upper crust, or the transmission of far-field stress through the elastic upper crust. These two mechanisms of stress transfer may not be easily discriminated from surface displacement fields recognized in geomorphic and geodetic studies (Gomberg and Ellis 1994).

The *en echelon* faults typical of strike–slip zones can be modeled as surfaces of discontinuity that produce a neighboring displacement field using dislocation theory, but with no interaction between the faults (Rodgers 1980) (Fig. 6.20b). The faults can also be viewed as large-scale fractures that interact to produce a local stress field (Segall and Pollard 1980). Two-dimensional plane stress models for pull-apart basins such as the latter calculate the strain around two *en echelon* fault tips in an elastic

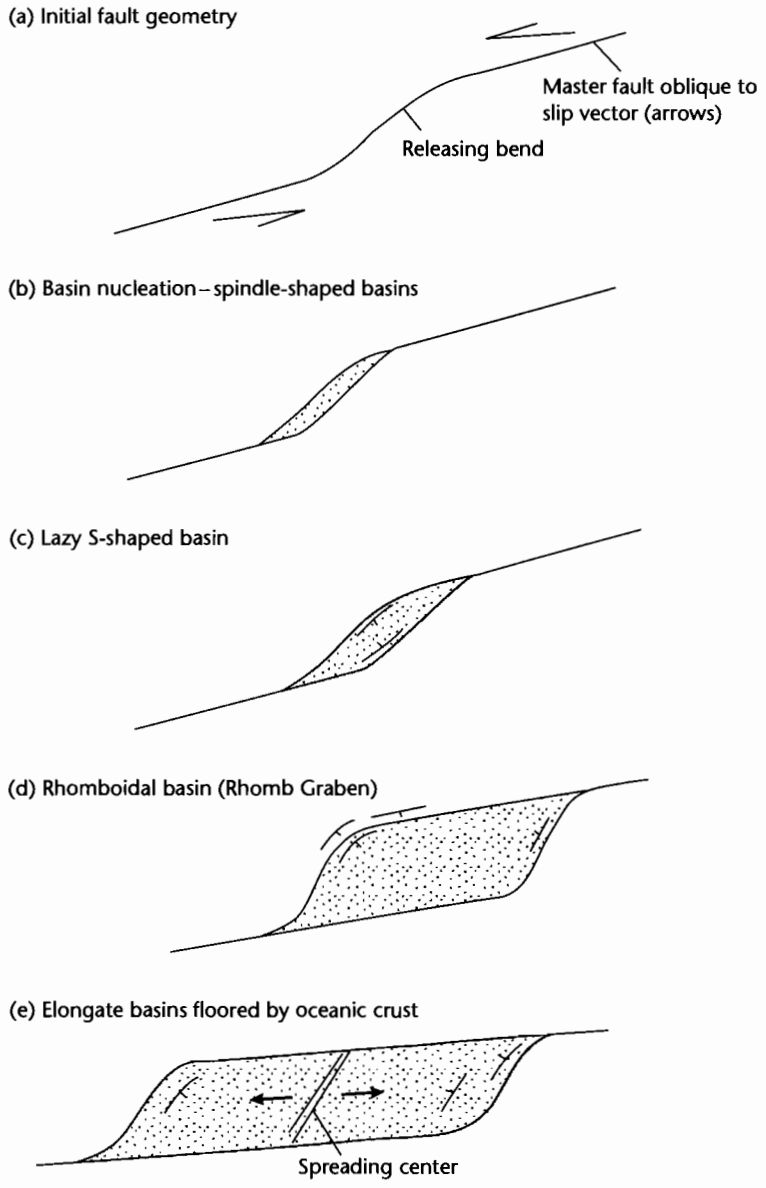

Fig. 6.19 Continuum model of pull-apart development, after Mann et al. (1983). (a) Pull-apart begins life on a releasing fault bend. The size of the bend controls the pull-apart basin width; (b) Spindle-shaped basin. Continued offset produces lazy S-shaped basin (c), then a rhomb-shaped basin (d), then finally a long, elongate trough floored with oceanic crust (e). Most pull-aparts do not reach the stage represented by (e). Instead they tend to be terminated after the basin length has reached about three times the original width of the releasing bend (or fault separation).

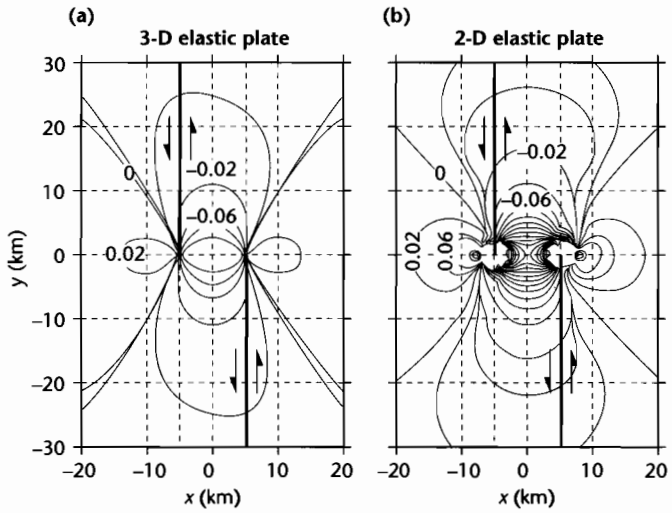

Fig. 6.20 Comparison between 2-D and 3-D plane stress models for pull-apart basins (after Katzman et al. 1995). A sinistral displacement discontinuity of 1 km is defined across two *en echelon* strike–slip faults. Vertical displacement is shown for (a) a 3-D elastic plate and (b) a 2-D thin elastic plate with elastic thicknesses of 15 km. Contour interval 0.02 km, Poisson's ratio 0.25 and Young's modulus 75 GPa. The 2-D plane stress model produces unrealistic deformation around the fault tips. Reproduced courtesy of American Geophysical Union.

medium. The 2-D plane stress model produces unrealistic, deep depocenters adjacent to the fault tips characterized by very high subsidence rates, together with unrealistic vertical uplifts above the fault tip. This results from the plane stress approximation, which does not allow stresses to develop in the vertical direction within the plate; consequently, stresses cannot resist deformation near the fault tips. The advantage of a 3-D model is that vertical stresses near the fault tips resist deformation, which dampens subsidence and uplift patterns in this region (Fig. 6.20a).

In the 3-D linear elastic model proposed by Katzman et al. (1995), the deformation is driven by a shear from below to simulate relative plate motion. The upper crust (*c.* 15 km) is penetrated fully by faults, that detach above the weak lower crust. Pull-apart basins develop close to two *en echelon* vertical faults 150 km long, spaced 10 km apart, with 0–20 km overlap (Fig. 6.21). The shear zone at the base of the plate is allowed to vary between 10 and 40 km. Two geometrical factors have important effects on pull-apart basin development:

1 *Shear zone width*: the basal shear causes slip to taper towards the fault tips, the rate of tapering decreasing with wider shear zones. As the shear zone width increases, the basin widens, lengthens and becomes shallower. Although the surface deformation varies strongly as a function of the shear zone width, the necking profiles in cross-section do not significantly vary.

2 *Fault overlap*: full graben develop between the overlapping faults over the entire overlap zone, becoming half-graben just outside the overlapping zone. Uplift decreases with the amount of overlap, reducing to zero at an overlap of *c.* 20 km. Less overlap causes greater rotation about a vertical axis.

The Dead Sea Basin is an ideal test for this 3-D numerical model. It is located along the left-lateral Dead Sea Transform at the plate boundary between the African and Arabian Plates (Garfunkel et al. 1981; Aydin and Nur 1982). The basin is narrow (*c.* 7–18 km), deep (*c.* 10 km), roughly symmetric, and extends along the strike of the bounding faults for 132 km (Fig. 6.22). Gravity and seismic reflection data (ten Brink and Ben-Avraham 1989) show that the Moho is not elevated beneath the basin. It is therefore thought to be uncompensated isostatically (as you would expect from the *c.* 10 km wavelength – see §2.3.3). The flanks of the basin are not topographically elevated compared to the regional

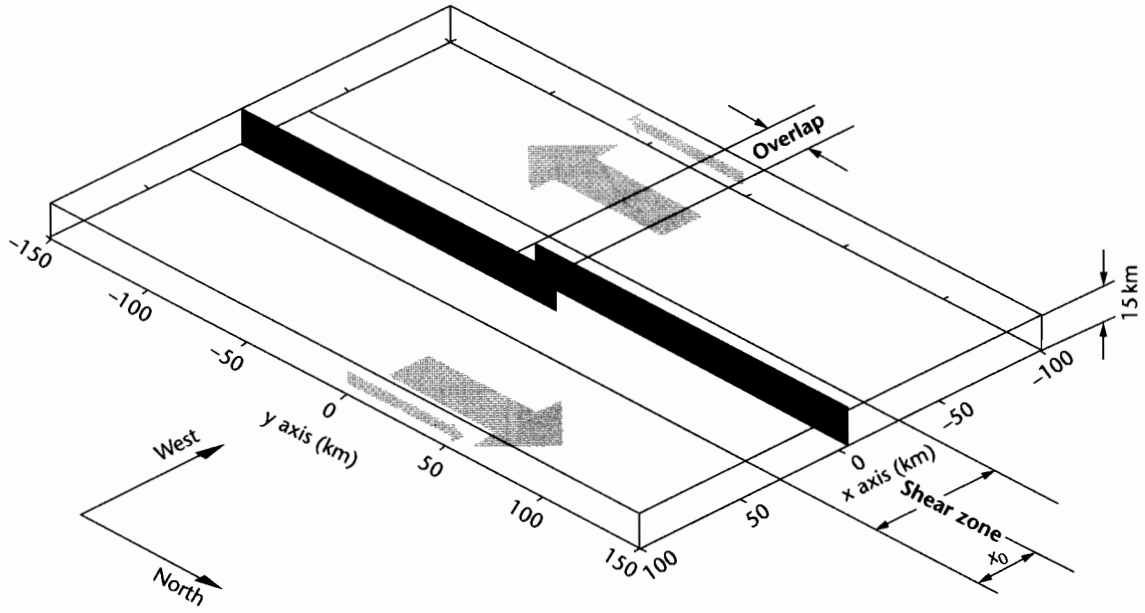

Fig. 6.21 Three-D block diagram showing the set up for the numerical pull-apart basin model (Katzman et al. 1995). Shaded planes define zones of weakness having zero shear strength (faults). Shaded arrows indicate the displacements defined as boundary conditions. The base of the model in the vicinity of the faults (within the shear zone) is stress free and thus freely deforming. The total width of the shear zone, $2x_0$, and the overlap distance between the fault segments, are varied in the model. Reproduced courtesy of American Geophysical Union.

elevation. The Dead Sea Basin is subsiding over a wide area, over several tens of kilometers in length. The extent of the basin subsidence is in harmony with the model predictions using 20–40 km-wide shear zones. However, the symmetric full-graben nature of the basin over a 50 km N–S distance, and the lack of topographic uplifts suggest that fault overlap must be greater than 20 km (twice the fault spacing). Katzman et al. (1995) suggested that the overlap distance increased during basin development.

6.3.4 Application of uniform extension model to pull-apart basins

The local extension in pull-apart basins causes very rapid subsidence and sediment accumulation, over 10 km of sediments accumulating in a period of less than 5 Myr in some examples such as the Miocene Ridge Basin of California (Link and Osborne 1978). The subsidence can be approximated by a model of lithospheric extension (McKenzie 1978a, §3.4.1), in which fault-controlled subsidence is followed by a thermal subsidence phase. Late Paleozoic pull-apart basins of eastern Canada (such as the 100 × 200 km Magdalen Basin, Gulf of St Lawrence area) are thought to have undergone a rift, then thermal subsidence history (Bradley 1983). However, the small size of pull-aparts implies that lateral temperature gradients must be large. Lateral heat conduction to the basin walls becomes an important source of heat loss, the narrower the basin the greater the cooling. The critical basin width below which lateral heat loss to the sides becomes important appears to be about 100 km (Steckler 1981) to 250 km (Cochran 1983). In comparison, most strike–slip basins are 10–20 km in width. Since narrow basins cool rapidly during extension, the subsidence is greater than predicted for the rift stage by the uniform extension model (§3.4.1). Rapid early subsidence related to lateral heat loss may help to explain the sediment starvation and deep bathymetries characteristic of the early

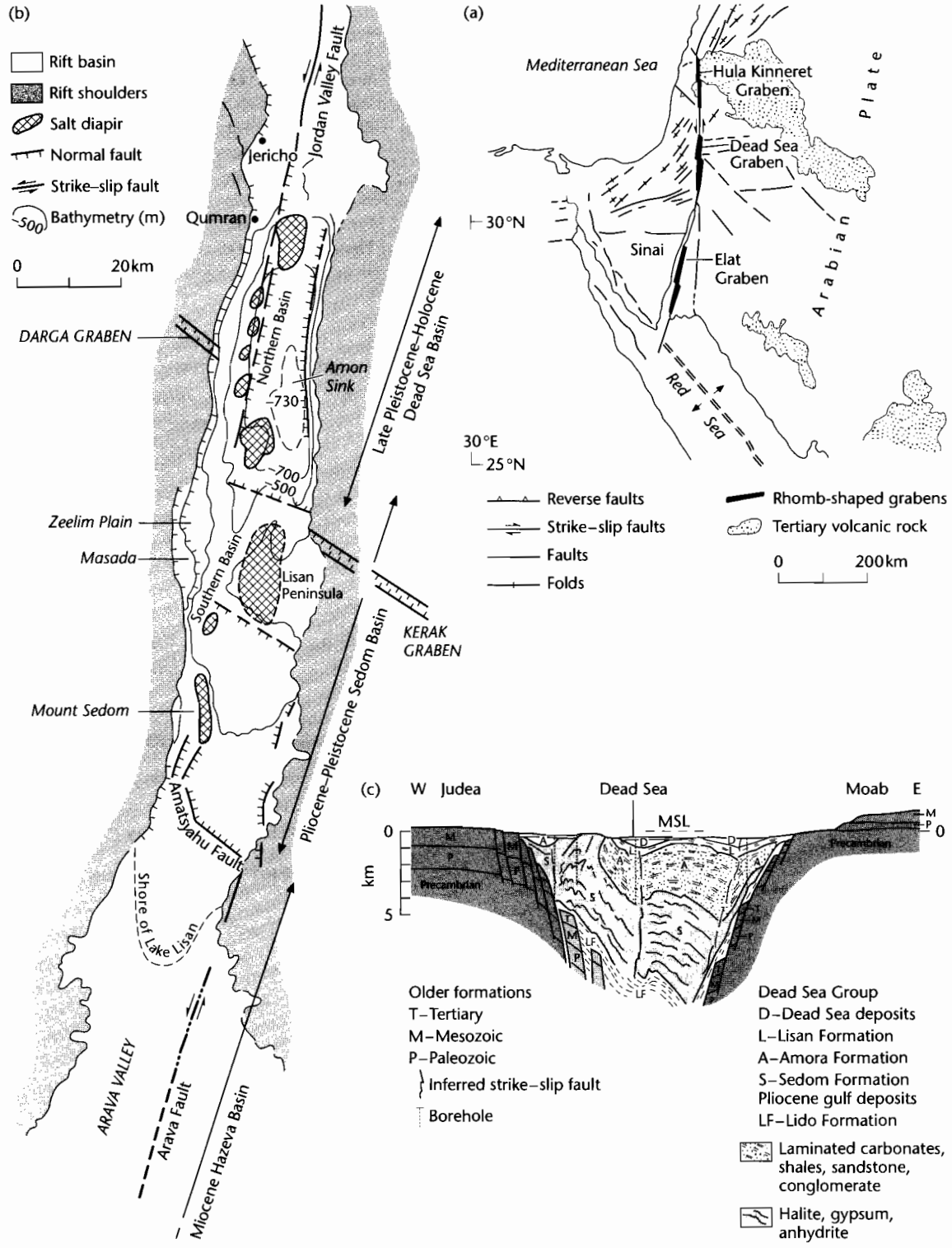

Fig. 6.22 (a) Location of Dead Sea Basin; (b) Structural interpretation, showing main faults, basins, and salt diapirs; (c) Cross-section of Dead Sea Basin between Mount Sedom and Moab. After ten Brink et al. (1993) and Katzman et al. (1995).

phases of pull-apart basin development. The subsequent postrift thermal subsidence should be correspondingly less.

Pitman and Andrews (1985) studied the subsidence history of small pull-aparts typical of the San Andreas zone of California. Here, thermal history and seismic data and geological studies (e.g., Atwater 1970) suggest an anomalously thin lithosphere in the mid to late Tertiary. In their model, the lithosphere was successively rifted then cooled over small time steps of 0.05 Myr to simulate the process of syn–rift heat loss (see also §3.5.3). For a basin filled with water only, the results of the model for a point in the center of the basin are shown in Figure 6.23a. The rapid initial subsidence is caused by faulting during crustal thinning combined with lateral heat loss to the basin walls. This steep curve flattens abruptly as extension terminates and the remaining subsidence is attributed to cooling only. Clearly, the initial basin width has a major influence on the subsidence history, the narrowest basins losing heat most rapidly to the sides and therefore subsiding both at a greater rate and with a greater magnitude than wider basins.

If the basin is kept at all times full to the brim, the subsidence must increase due to isostasy by a factor related to the different densities of water and infilling sediment $[(\rho_m - \rho_w)/(\rho_m - \rho_s)]$. Pitman and Andrews (1985) suggested that in the early stages of basin development, the sediment supply rate from uplifting and eroding catchments will not keep pace with tectonic subsidence, thereby explaining the starved youthful stages of many pull-apart basins. The basin should gradually fill as the subsidence rate slackens, eventually filling completely some 5 Myr after the start of rifting (Fig. 6.23b). The Tekirdag Depression along the North Anatolian Fault has been active in the Pliocene–Quaternary and has a basin

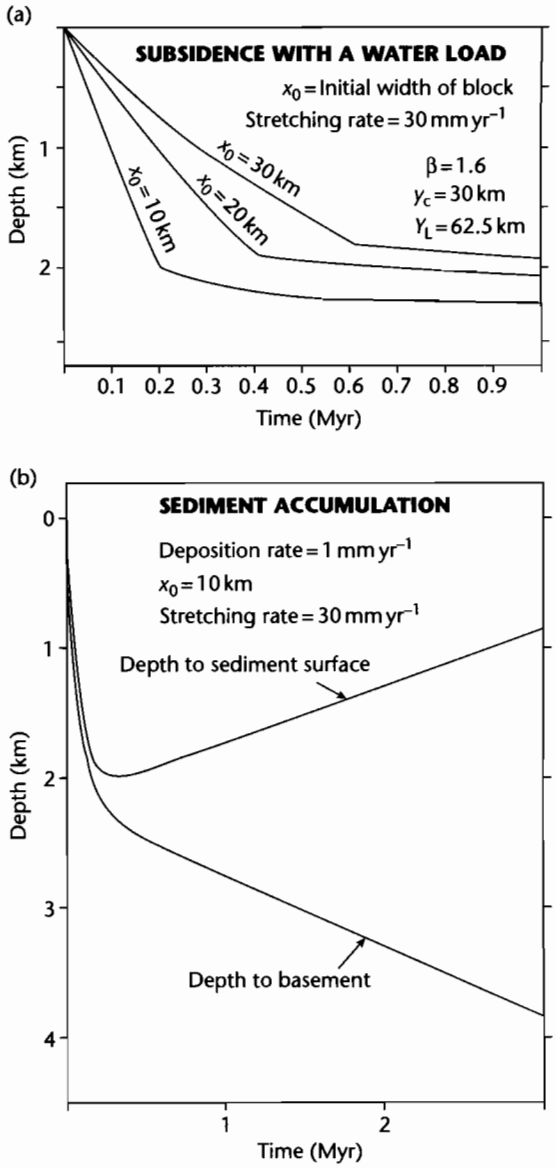

Fig. 6.23 (a) Subsidence as a function of time for basins experiencing lateral heat loss in addition to vertical conduction. Three subsidence curves are shown for three initial widths of zones of stretching (10, 20, and 30 km) for a point in the centre of the basin. The initial lithospheric thickness is 62.5 km. The infilling medium is assumed to be water. The crustal blocks are stretched at 30 mm yr^{-1} up to a stretch factor of 1.6. The curves comprise two segments. The initial steep segment represents subsidence due to lateral heat loss as well as crustal stretching. The flatter later segment represents subsidence due to the remaining thermal contraction. The total subsidence and the time history of subsidence are both influenced by the initial width of the zone of stretching between unstretched basin walls; (b) The depth to basement and the depth to the sediment surface in a narrow (initially 10 km-wide) basin characterized by lateral heat loss where the rate of sediment supply is restricted to 1 mm yr^{-1}. Local (Airy) isostasy is assumed throughout in compensating the depth to basement for the sediment load. The early history of the basin is marked by deep water sedimentation and several million years elapse before the sediment surface approaches sea level. Such a stratigraphic evolution is found, for example, in the Ridge Basin of California. After Pitman and Andrews (1985).

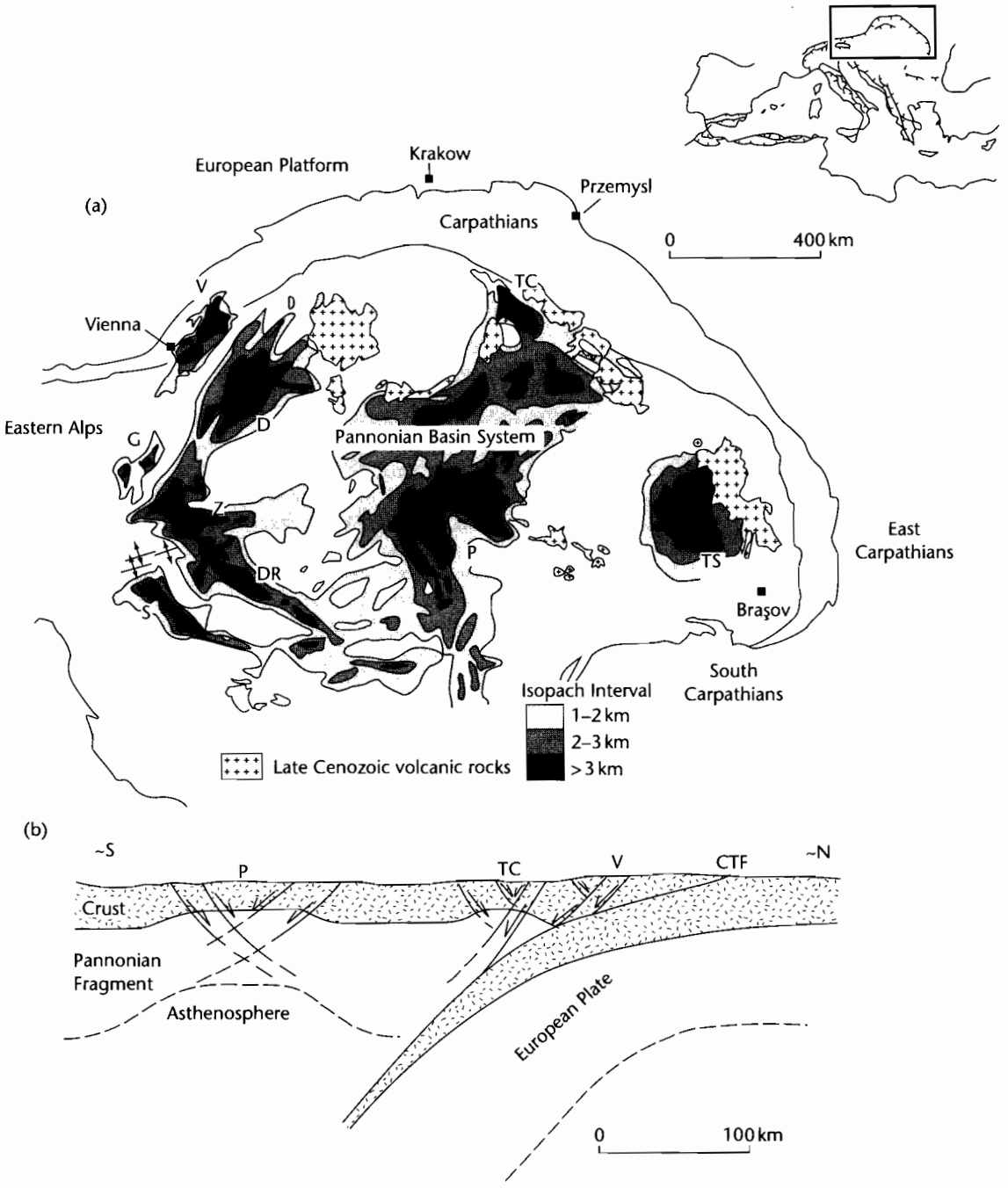

Fig. 6.24 Map (a) and schematic cross-section (b) to show the relationship between the Vienna Basin to other basins in the Carpathian–Pannonian system. The Vienna Basin is situated at a left step (releasing bend) in a sinistral strike–slip system accommodating relative movement between active and inactive nappes in the Alpine–Carpathian orogenic system. The Vienna and Transcarpathian Basins are located on the leading (thin) edge of the Pannonian lithosphere and above the deflected European Plate. The Pannonian Basin, however, is located entirely on the Pannonian lithosphere where it overlies asthenosphere. Extension in the Pannonian Basin therefore involves mantle and the basin is consequently "hot" compared to the "cool" Vienna Basin (Royden 1985). CTF, Carpathian Thrust Front; V, Vienna Basin; P, Pannonian Basin; TC, Transcarpathian Basin; TS, Transylvanian Basin; S, Sava Basin; DR, Drava Basin; D, Danube Basin; G, Graz Basin; Z, Zala Basin.

floor at maximum depths of 1150 m, suggesting that basin subsidence has far outstripped sediment supply for the last <4 Myr (Okay et al. 1999). The Ridge Basin of California was initiated in the Late Miocene and was initially occupied by a deep marine embayment before continental conditions prevailed in the Pliocene (Link and Osborne 1978). These two examples therefore support the idea of early underfilled stages in pull-apart basins caused by high subsidence rates.

6.3.5 Detached pull-apart basins in regions of lithospheric compression

It has previously been observed that the common block rotations in zones of strike–slip deformation require a detachment beneath the brittle upper crust. The stretching of the upper crust without associated mantle upwelling is suggested by the generally low heat flows of many strike–slip zones. The narrowness of strike–slip basins, and of the topographic features associated with strike–slip deformation, indicate that they are essentially uncompensated isostatically. We refer to such cases as thin-skinned strike–slip basins. Thin-skinned strike–slip basins should exhibit a distinctive subsidence and thermal history compared to basins involving mantle upwelling. Detachments beneath the upper crust may be related to lithospheric extension or to lithospheric convergence. The Vienna Basin of Austria is an example of the latter.

The 200 km by 60 km Vienna Basin contains up to 6 km of Miocene sedimentary rocks and formed adjacent to the coeval Carpathian thrust belt. The Vienna Basin is an excellent example of a rhombohedral pull-apart that developed on top of the allochthonous thrust terranes of the Alpine–Carpathian system in a background environment of lithospheric shortening (Fig. 6.24). The NE–SW trending major fault systems active during sedimentation in the Vienna Basin do not significantly disrupt the underlying autochthonous cover rocks of the European Plate and appear to pass into flat detachments using older thrust planes (Royden 1985).

An important observation in explaining the Vienna Basin is that the thrust sheets west of the Vienna Basin became fixed at the end of the early Miocene whilst thrusting continued east of the basin (Fig. 6.24). This relative displacement requires either: (i) sinistral bending of the thrust belt near the Vienna Basin, or the preferred case, (ii) left-slip along N or NE striking faults within the thrust belt. Thus, the Vienna Basin can be viewed as a result of diachronous thrusting in a region of oblique convergence.

If the Vienna Basin is essentially thin-skinned (<10 km), it has considerable implications for the subsidence and thermal history of this variety of pull apart basin. Since the extension is thin-skinned, the lower crust and mantle should be unaffected by the extension near the surface. This is supported by a number of lines of evidence: (i) the uniformly low heat flows of 45–60 $mW\,m^{-2}$ through the Vienna Basin and adjacent regions (Cermak 1979; Royden 1985), (ii) subsidence curves derived from boreholes show no recognizable thermal subsidence phase, and (iii) low thermal gradients and low levels of organic maturity. This contrasts strongly with strike–slip basins with involvement of the lower crust and mantle lithosphere. Such basins, like the neighboring Pannonian Basin (Fig. 6.24), have much higher geothermal gradients and correspondingly high levels of organic maturity.

Basins such as the Vienna Basin with shallow detachments may be typical of zones close to the thrust front. As the distance from the thrust front increases, extension may reach progressively greater depths, ultimately affecting the entire lithosphere. This may explain why the Pannonian Basin situated far to the south of the arcuate Carpathian suture involves mantle extension (Fig. 6.24) and elevated heat flows, whereas the Vienna Basin located within the Carpathian system is extremely thin-skinned and consequently cool, with no postextension thermal subsidence.